

 Open access • Posted Content • DOI:10.1101/2021.05.24.445445

## Dissection of multiple sclerosis genetics identifies B and CD4 T cells as driver cell subsets — [Source link](#)

Michael H. Guo, Michael H. Guo, Prashanth Sama, Brenna A. LaBarre ...+12 more authors

**Institutions:** Massachusetts Institute of Technology, University of Pennsylvania, Brigham and Women's Hospital

**Published on:** 25 May 2021 - bioRxiv (Cold Spring Harbor Laboratory)

**Topics:** Chromatin, Epigenetics and Cell type

Related papers:

- [Integrated single-cell transcriptomics and epigenomics reveals strong germinal center-associated etiology of autoimmune risk loci](#)
- [Single cell chromatin accessibility reveals pancreatic islet cell type- and state-specific regulatory programs of diabetes risk](#)
- [Dense module searching for gene networks associated with multiple sclerosis.](#)
- [Virtual Sorting Has a Distinctive Advantage in Identification of Anticorrelated Genes and Further Negative Regulators of Immune Cell Subpopulations.](#)
- [A transcriptome-based approach to identify functional modules within and across primary human immune cells.](#)

Share this paper:    

View more about this paper here: <https://typeset.io/papers/dissection-of-multiple-sclerosis-genetics-identifies-b-and-2p9tamyqo0>

1 **Title: Dissection of multiple sclerosis genetics identifies B and CD4+ T cells as driver cell**  
2 **subsets**

3  
4 Michael H. Guo, MD, PhD<sup>1,2\*</sup>; Prashanth Sama<sup>2-5</sup>, MSc; Brenna A. LaBarre, PhD<sup>2-5</sup>, Hrishikesh<sup>6-</sup>  
5 <sup>7</sup> Lokhande, MSc, John Balibalos<sup>8</sup>, Ci Chu, PhD<sup>8</sup>, Xiaomi Du<sup>8</sup>, Pouya Kheradpour, PhD<sup>8</sup>,  
6 Charles C Kim, PhD<sup>8</sup>, Taylor Oniskey<sup>8</sup>, Thomas Snyder, PhD<sup>8</sup>, Damien Z Soghoian, PhD<sup>8</sup>,  
7 Howard L. Weiner, MD<sup>6-7</sup>, Tanuja Chitnis, MD<sup>6-7</sup>, Nikolaos A. Patsopoulos, MD, PhD<sup>2-5\*</sup>

- 8 1. Department of Neurology, Perelman School of Medicine, University of Pennsylvania,  
9 Philadelphia, Pennsylvania, USA.  
10 2. Broad Institute of Harvard and Massachusetts Institute of Technology, Cambridge, MA, USA  
11 3. Systems Biology and Computer Science Program, Ann Romney Center for Neurological  
12 Diseases, Department of Neurology, Brigham & Women's Hospital, Boston, 02115 MA, USA  
13 4. Division of Genetics, Department of Medicine, Brigham & Women's Hospital, Harvard  
14 Medical School, Boston, MA, USA.  
15 5. Harvard Medical School, Boston, MA 02115, USA.  
16 6. Brigham Multiple Sclerosis Center, Brigham and Women's Hospital, Boston, Massachusetts,  
17 USA.  
18 7. Ann Romney Center for Neurologic Diseases, Brigham and Women's Hospital, Boston,  
19 Massachusetts, USA.  
20 8. Verily Life Sciences, South San Francisco, 94080

21  
22 \*Corresponding authors

23 Correspondence should be addressed to:

24 Nikolaos Patsopoulos, [npatsopoulos@rics.bwh.harvard.edu](mailto:npatsopoulos@rics.bwh.harvard.edu)

25 Michael Guo, [michael.guo@penncmedicine.upenn.edu](mailto:michael.guo@penncmedicine.upenn.edu)

26 Target Journal: Nature Communications

27 Word Count (without Methods): 5174

28 Word count, Methods: 2305

29 Figures: 8

30 Supplementary material: 29 Supplementary Tables, 17 Supplementary Figures

31 Abstract: 151

32 References: 57

33 **Abstract**

34 Multiple sclerosis (MS) is an autoimmune condition of the central nervous system with a well-  
35 characterized genetic background. Prior analyses of MS genetics have identified broad  
36 enrichments across peripheral immune cells, yet the driver immune subsets are unclear. We  
37 utilized chromatin accessibility data across hematopoietic cells to identify cell type-specific  
38 enrichments of MS genetic signals. We found that CD4 T and B cells were independently  
39 enriched for MS genetics and further refined the driver subsets to T<sub>h</sub>17 and memory B cells,  
40 respectively. We replicated our findings in data from untreated and treated MS patients and  
41 found that immunomodulatory treatments suppress chromatin accessibility at driver cell types.  
42 Integration of statistical fine-mapping and chromatin interactions nominated numerous putative  
43 causal genes, illustrating complex interplay between shared and cell-specific genes. Our study  
44 highlights how careful integration of genetics and epigenetics can provide fine-scale insights into  
45 causal cell types and nominate new genes and pathways for disease.

## 46 **Introduction**

47 Multiple sclerosis (MS) is an immune-mediated neurodegenerative disease characterized by  
48 demyelinating focal lesions in the central nervous system (CNS)<sup>1</sup>. Despite the CNS being the  
49 target of autoimmunity, there is extensive evidence from basic science models and human  
50 studies that dysregulation of the peripheral immune compartment is key for disease  
51 manifestation and progression<sup>2</sup>. MS has long been regarded as a T cell-mediated disease, with  
52 several T cell subpopulations implicated<sup>3,4</sup>. More recently, other peripheral immune cell  
53 populations, most notably B cells, have also been shown to drive disease pathogenesis<sup>3,5</sup>.  
54 Moreover, immune modulating therapies targeting B cells have been demonstrated to be  
55 remarkably effective in treating patients with MS<sup>6,7</sup>.

56  
57 MS has a strong genetic component and is characterized by a polygenic architecture. To date,  
58 over 200 independent genetic variants have been associated with MS risk, the vast majority of  
59 which are common variants with small effect sizes on disease risk<sup>8,9</sup>. Prior studies have shown  
60 enrichment of GWAS target genes in the peripheral immune system, but it is unclear exactly  
61 which cell types within the peripheral immune system drive these observed enrichments of  
62 genetic signals.

63  
64 Human genetics has emerged as a powerful tool for probing the underlying biology of a  
65 disease<sup>10</sup>. The identification of genes and pathways prioritized by GWAS associations is not  
66 constrained by our prior knowledge of disease mechanisms and can therefore identify novel  
67 biological mechanisms. However, a key challenge for translating GWAS findings into biological  
68 insights is that most associations are noncoding in nature and likely act by modulating  
69 regulatory elements to mediate gene expression<sup>11,12</sup>. Identifying the causal gene at these  
70 GWAS signals can be challenging since it is usually unclear which gene a given regulatory  
71 element regulates<sup>10,13,14</sup>. A key step in translating genetic associations into biological

72 mechanisms is identifying the cell types in which GWAS variants act and the genes they  
73 modulate. To help understand the function of disease-associated variants, genetic associations  
74 can be intersected with orthogonal epigenetic and gene expression data<sup>12</sup>. As the epigenetic  
75 and gene expression landscape differ from cell type to cell type, examining the enrichments of  
76 GWAS data on these orthogonal datasets can identify specific cell types that may be implicated  
77 in disease pathogenesis<sup>15,16</sup>.

78  
79 We and others have previously reported a strong enrichment of MS GWAS variants in  
80 regulatory regions of multiple cell types of the peripheral immune system<sup>8,9,15,17</sup>. However, it has  
81 yet to be determined if these enrichments are driven by shared regulatory mechanisms common  
82 to many immune cell types, or whether different mechanisms are present in distinct immune cell  
83 populations. To address this gap, we performed detailed analyses of the enrichment of MS  
84 GWAS variants in the peripheral immune system to identify cell populations that independently  
85 mediate the effects of MS GWAS variants on disease risk.

86

## 87 **Results**

### 88 *MS GWAS associations are enriched in progenitor and terminal peripheral immune cells*

89 To identify the causal cell types that uniquely and independently contribute to MS pathogenesis  
90 via mediation of genetic effects, we leveraged bulk ATAC-seq data from 16 flow-sorted  
91 hematopoietic progenitor and terminal cell populations isolated from human peripheral blood or  
92 bone marrow<sup>18–20</sup>. These cells represent progenitor and terminal populations from across the  
93 hematopoietic tree, enabling investigation of MS GWAS enrichments broadly and across stem,  
94 progenitor, and mature cell populations (**Figure 1A**). ATAC-seq data were processed and open  
95 chromatin regions (OCRs, i.e. ATAC-seq peaks), were identified as previously described<sup>18,21</sup>.  
96 We applied stratified LD Score regression (LDSC)<sup>22,23</sup> to estimate the enrichment of MS GWAS

97 in OCRs from each of the 16 hematopoietic cell types. LDSC has the distinct advantage in that it  
98 leverages the genome-wide polygenic signal in the GWAS summary statistics rather than  
99 selecting variants based on p-value thresholds or fine-mapping posterior probabilities.

100  
101 Applying LDSC, we observed strong statistically significant enrichments across all  
102 hematopoietic cell populations, even after correcting for multiple hypothesis testing (Bonferroni-  
103 corrected p-value threshold of  $3.13 \times 10^{-3}$ ) (**Figure 1B; Supplemental Table 1**). The strongest  
104 enrichments for MS GWAS were observed in OCRs from CD4 T cells (enrichment p-value =  
105  $1.47 \times 10^{-18}$ ), CD8 T cells (p-value =  $4.00 \times 10^{-18}$ ) and B cells (p-value =  $3.27 \times 10^{-15}$ ); reflecting their  
106 known and emerging roles in MS pathogenesis and as targets of treatment<sup>1,3,24</sup>. We also  
107 detected strong enrichment in OCRs from natural killer (NK) cells (p-value =  $4.23 \times 10^{-14}$ ) which  
108 have a less well-established role in MS<sup>24</sup>. Interestingly, we observed enrichments across all  
109 progenitor cells, suggesting that many MS genetic associations are located in regulatory regions  
110 involved in core cellular processes in immune cell populations.

111

### 112 *CD4 T and B cell regulatory regions independently mediate MS genetics*

113 Many of the studied cell populations share common cellular regulatory signatures, which is  
114 reflected in the substantial correlation of the OCR profiles across cell populations (**Figure S1**).  
115 Hence, we examined whether the strong enrichment observed across cell populations is a result  
116 of truly independent cell type-specific enrichments or whether it is due to shared regulatory  
117 landscape across immune cell types. To address this question, we applied a joint model in  
118 LDSC to measure the contribution of OCRs from a given cell type, stratified on all other cell  
119 types in the model along with a set of baseline annotations. We report the p-value of the  
120 coefficient  $\tau_c$ , which reflects the SNP heritability of a given annotation stratified on all other  
121 annotations in the model. In this joint model where OCRs from all 16 cell types were included,

122 we observed that B cells and CD4 T cells contributed significantly to SNP heritability (coefficient  
123 p-value =  $3.99 \times 10^{-5}$  and  $3.49 \times 10^{-4}$ , respectively), suggesting independent contributions of B and  
124 CD4 T cell OCRs to MS GWAS heritability (**Figure 2A, Supplemental Table 2**).

125  
126 To further delineate the cell types with OCRs that specifically mediate the effect of MS GWAS  
127 results, we performed a series of pairwise LDSC analyses. In brief, OCRs of a given  
128 hematopoietic cell type were stratified against the OCRs of each of the other 15 cell types, as  
129 well as the LDSC baseline annotations (**Figure 2B; Supplemental Table 3**). As above with the  
130 joint model, we report the p-value of the coefficient  $\tau_c$ . We observed that B cells remained  
131 significant even after stratifying on OCRs of any of the other 15 cell populations (coefficient p-  
132 value ranging from  $1.47 \times 10^{-12}$  when stratifying against HSCs, to  $8.33 \times 10^{-5}$  when stratifying  
133 against CD4 T cells). This was also the case for CD4 T cells, which remained significant after  
134 stratifying on OCRs from any of the other 15 cell populations (coefficient p-values ranging from  
135  $3.82 \times 10^{-17}$  when stratifying against HSCs, to  $2.39 \times 10^{-4}$  when stratifying against CD8 T cells). In  
136 contrast, CD8 T cell OCRs were no longer significant after stratifying against OCRs from CD4<sup>+</sup>  
137 T cells (coefficient p-value = 0.21), though they were significant when stratifying on any of the  
138 other cell populations. NK cells were also no longer significant after stratifying against either  
139 CD4 T cells (coefficient p-value = 0.165) or against CD8 T cells (coefficient p-value: 0.356).  
140 These results indicate that the enrichment of both CD8 T cells and NK cells can be largely  
141 explained by shared regulatory landscapes that are also present in CD4 T cells. Prior studies  
142 have also suggested a role for monocytes in MS<sup>24,25</sup>. OCRs from monocytes had an enrichment  
143 p-value of  $4.17 \times 10^{-9}$ , but we observed that stratifying on OCRs from CD4 T cells or B cells  
144 ameliorated this monocyte heritability enrichment (coefficient p-values 0.166 and 0.266,  
145 respectively).

146

147 We also performed a separate analysis examining whether OCRs specific to a given cell type  
148 mediate MS heritability enrichments. For each of the mature hematopoietic cell populations, we  
149 performed LDSC on only the cell type-specific OCRs, i.e. ATAC-seq peaks present in only that  
150 cell type. B cells exhibited a statistically significant enrichment of cell-specific OCRs for MS  
151 GWAS (enrichment p-value =  $3.27 \times 10^{-4}$ ). CD4 T cell-specific peaks were nominally significant at  
152 a p-value of 0.013 but did not survive correction for multiple hypothesis testing (Bonferroni  
153 corrected p-value threshold of  $5.6 \times 10^{-3}$ ). Cell type-specific peaks for all other terminal  
154 hematopoietic cell types had enrichment p-values  $> 0.05$  (**Figure S2; Supplementary Table 4**).  
155

### 156 *MS genetic associations are mediated in terminal immune cell populations*

157 In the lymphoid lineage, we observed stronger enrichments in terminal cell populations than we  
158 did for the progenitor populations (**Figure 1B**). For example, the strongest enrichment in  
159 progenitor cells was observed for common lymphoid progenitor cells (CLP, enrichment p-value:  
160  $2.32 \times 10^{-4}$ ), and it was orders of magnitude less statistically significant compared to the  
161 enrichment observed for CD4 T or B cells (**Figure 1B**). For each of the terminal populations, the  
162 significance remained even after stratifying against OCRs from CLP; however, the converse  
163 was not true (**Figure 2B**). The enrichment in CLP was completely ameliorated by stratifying  
164 against B cell or CD4 T cell OCRs (coefficient p-value 0.98 and 0.966, respectively, **Figure 2B**).  
165 Together, these results suggest that terminal cells of the lymphoid compartment retain cellular  
166 regulatory features from their progenitor populations that are important for MS pathogenesis, but  
167 have also developed specific regulatory features of additional importance to MS susceptibility.  
168

### 169 *Comparison of immune cell enrichment with neuropsychiatric and autoimmune disorders*

170 We next sought to understand how the immune cell enrichments in MS might be similar or  
171 different from those of other autoimmune or neuropsychiatric disorders. To test this, we



172 calculated heritability enrichment within these 16 hematopoietic OCRs for GWAS of various  
173 other neuropsychiatric disorders and autoimmune disorders: Alzheimer disease (AD)<sup>26</sup>,  
174 schizophrenia (SCZ)<sup>27</sup>, bipolar disorder (BPD)<sup>28</sup>, type 1 diabetes (T1D)<sup>29</sup>, Crohn's disease  
175 (CD)<sup>30</sup>, ulcerative colitis (UC)<sup>30</sup>, systemic lupus erythematosus (SLE)<sup>31</sup>, rheumatoid arthritis  
176 (RA)<sup>32</sup>, and primary biliary cirrhosis (PBC)<sup>33</sup> (**Figure 3A; Supplemental Table 5**). We identified  
177 previously recognized cell-type enrichments across these other diseases, such as enrichments  
178 in OCRs from B cells (enrichment p-value:  $1.93 \times 10^{-7}$ ), CD4 T cells (p-value:  $7.34 \times 10^{-8}$ ) and CD8  
179 T cells (p-value:  $2.09 \times 10^{-6}$ ) for RA<sup>15,32</sup>. However, the heritability enrichments for OCRs from  
180 these hematopoietic cell populations tended to be much stronger for MS, despite similar sample  
181 sizes, e.g. 41,505 disease cases for MS and 38,242 disease cases for RA. To parse out cell  
182 type-specific enrichments in these other disorders, we also tested heritability enrichments under  
183 the joint model in LDSC by including OCRs from all 16 cell types (**Figure 3B, Supplemental**  
184 **Table 6**). In a similar fashion to the MS GWAS joint analyses above, we measured the  
185 contribution to heritability for a given set of OCRs of interest, controlling for the effects of a set of  
186 baseline annotations and OCRs from all other hematopoietic cell types. These analyses were  
187 performed separately for each disease. Across the nine other comparator diseases, the only  
188 other statistically significant stratified enrichments were in OCRs from B cells in SLE GWAS  
189 (coefficient p-value:  $8.53 \times 10^{-5}$ ). We also identified other enrichments in this joint model that were  
190 nominally significant, including signals for several diseases in either B or CD4 T cells. This is in  
191 contrast to our MS findings, which show strong enrichments in both CD4 T cells and B cells,  
192 highlighting a dual role of these cell types in MS and distinguishing it from other diseases where  
193 the cell types are more restricted to specific lineages.

194

195 *The CD4 T cell MS GWAS enrichment is driven by the Th17 subset*

196 To further focus in on the MS GWAS enrichment observed in OCRs from CD4 T cells, we  
197 utilized ATAC-seq data from various subsets of human CD4 T cells (**Figure 4A**)<sup>21</sup>. We examined  
198 data from effector CD4 T cells (naïve effector CD4 T cells, T<sub>h</sub>1, T<sub>h</sub>2, T<sub>h</sub>17, and follicular T<sub>h</sub>) as  
199 well as, regulatory CD4 T cells (naïve T<sub>regs</sub> and memory T<sub>regs</sub>). We observed strong enrichments  
200 for OCRs from both effector and regulatory CD4 T cell populations (**Figure 4B; Supplementary**  
201 **Table 7**). Next, to identify the independent contribution of a given cell type, we applied the joint  
202 model in LDSC by including OCRs from all CD4 T cell populations together. This joint LDSC  
203 analysis revealed that OCRs from T<sub>h</sub>17 cells independently contributed to heritability (coefficient  
204 p-value = 4.69x10<sup>-4</sup>; **Figure 4C; Supplemental Table 8**). Performing pairwise stratified LDSC  
205 confirmed the independent contribution of OCRs in T<sub>h</sub>17 cells to MS GWAS heritability (**Figure**  
206 **4D; Supplemental Table 9**). OCRs from T<sub>h</sub>17 remained enriched in MS GWAS even after  
207 stratifying against any of the other T<sub>eff</sub> cell populations or T<sub>reg</sub> cell populations. Conversely, the  
208 enrichments for all other T<sub>eff</sub> cell populations or T<sub>reg</sub> cell populations were ameliorated when  
209 stratifying against T<sub>h</sub>17 cells.

210  
211 Based on the LDSC analyses in the joint model, we note that enrichments tended to be stronger  
212 in OCRs from the memory effector CD4 T cell populations than from naïve effector cells. For  
213 each of these memory effector CD4 T cell populations, OCRs retained statistical significance  
214 even after stratifying against OCRs from naïve T<sub>eff</sub> cells: T<sub>h</sub>1 (coefficient p-value after stratifying  
215 against naïve T<sub>eff</sub> cells: 8.22x10<sup>-6</sup>), T<sub>h</sub>2 (p-value = 1.45x10<sup>-4</sup>), T<sub>h</sub>17 (p-value = 7.27x10<sup>-7</sup>) or  
216 follicular T<sub>h</sub> cells (p-value = 1.77x10<sup>-7</sup>) (**Figure 4D**). The converse was not true; the statistical  
217 significance of the naïve T<sub>eff</sub> cell OCRs was completely lost when stratifying against OCRs from  
218 any of the memory T<sub>eff</sub> cell populations. These results suggest that among CD4 T cells, OCRs  
219 from T<sub>h</sub>17 cells drive the signal for enrichment in MS GWAS.

220

221 *Memory subpopulations explain the enrichment of MS GWAS in B cells*

222 We next examined enrichments of MS GWAS data in ATAC-seq from the B cell lineage  
223 including naïve B cells, memory B cells, and plasmablasts (**Figure 5A**)<sup>21</sup>. We found that OCRs  
224 from all B cell lineage cell types were significantly enriched for MS heritability (**Figure 5B**;  
225 **Supplemental Table 10**). LDSC under a joint model including all B cell lineage cell types  
226 revealed an independent contribution from memory B cells (coefficient p-value =  $1.10 \times 10^{-3}$ ),  
227 but not naïve B cells or plasmablasts **Figure 5C**; **Supplemental Table 11**). Pairwise stratified  
228 LDSC confirmed the independent enrichment of OCRs from memory B cells. Memory B cell  
229 OCRs remained statistically significant even after stratifying on naïve B cells (coefficient p-value  
230 =  $1.26 \times 10^{-5}$ ) or plasmablasts (coefficient p-value:  $3.29 \times 10^{-4}$ ; **Figure 5D**; **Supplemental Table**  
231 **12**). In contrast, OCRs from naïve B cells and plasmablasts were no longer statistically  
232 significant when stratifying on memory B cells OCRs (coefficient p-value: 0.71 and 0.27,  
233 respectively). These results suggest that in the B cell lineage, the MS GWAS enrichment signal  
234 is driven by OCRs in memory B cells.

235

236 *Immune cells from MS patients reinforce independent CD4 T and B cell enrichments*

237 Next, we tested whether the MS GWAS enrichment in CD4+ T and B cells were also present in  
238 OCRs from the respective immune cell types derived from individuals with MS. We utilized  
239 ATAC-seq data performed in flow-sorted bulk CD4 T and B cell subsets (n=6) derived from six  
240 patients with MS who were not treated with immunomodulatory therapy within at least 4 months  
241 of sample collection (see **Supplementary Table 13** for clinical details). LDSC showed  
242 statistically significant enrichments of transitional B cells (traB; enrichment p-value= $2.08 \times 10^{-3}$ ),  
243 class switched classical memory B cells (cMBc; p-value =  $2.58 \times 10^{-4}$ ), effector memory CD4 T  
244 cells (T4<sub>em</sub>; p-value =  $1.87 \times 10^{-4}$ ), and CD45RA+ effector memory CD4 T cells (T4<sub>ra</sub>; p-value =  
245  $3.02 \times 10^{-4}$ ). Central memory CD4 T cells had an enrichment p-value of  $1.53 \times 10^{-3}$ , which was not

246 significant after correcting for multiple hypothesis testing (**Figure 6A; Supplementary Table**  
247 **14**).

248  
249 To further identify independent cell type enrichments, we performed joint models in LDSC as  
250 described above. We first tested a model that included CD4 T cell subsets (T4nv, T4cm, T4em,  
251 and T4ra). In this joint model, only T4em was statistically significant (coefficient p-value  $7.45 \times$   
252  $10^{-3}$ ), reflecting the independent contribution of effector CD4 T cells in MS that we observed  
253 above using cells from healthy individuals (**Figure 6B; Supplementary Table 15**). We also ran  
254 a model that included B cell subsets (traB and cMBc). In this joint comparison, neither cell type  
255 was statistically significant when correcting for multiple hypothesis testing. However, cMBc had  
256 a coefficient p-value that was nominally significant (p-value=0.037), reiterating the independent  
257 contributions of mature B cell types (**Figure 6C; Supplementary Table 16**).

258

### 259 *Immunomodulatory treatments suppress mediation of MS genetics in cell-specific fashion*

260 Next, we tested whether immunomodulatory treatments alter the cell-specific mediation of MS  
261 genetic associations by utilizing data for the same immune subsets sorted from patients with MS  
262 (n=3) under treatment with either natalizumab, interferon, or glatiramer acetate. Following  
263 treatment with any of the agents still resulted in statistically significant enrichments of cMBc and  
264 T4em (**Figure 6D; Supplementary Table 17**), though the magnitude of the enrichments were  
265 attenuated relative to the signals observed from cells from untreated patients (compare **Figure**  
266 **6A and 6D**). To better understand this attenuation of enrichments, we ran joint models in LDSC  
267 for T4em and cMBc cells in which we included OCRs from untreated patients and treated  
268 patients. In a joint model with T4em OCRs from treated and untreated MS patients, only OCRs  
269 from untreated patients were statistically significant (**Figure S3A; Supplementary Tables 18**).  
270 Similarly, in a joint model with cMBc OCRs from treated and untreated MS patients, only OCRs

271 from untreated patients were statistically significant (**Figure S3B; Supplementary Table 19**).  
272 Together, these results suggest that immune-modulating therapies may attenuate the chromatin  
273 accessibility signals at MS GWAS.

274

### 275 *MS GWAS signals in B and CD4 T cells driven by active enhancer and promoter regions*

276 We next sought to gain further insight into the functional consequences of the B and CD4 T cell  
277 OCRs underlying MS GWAS signals. We examined enrichments for MS GWAS in chromatin  
278 immunoprecipitation sequencing (ChIP-seq) peaks from various histone modifications  
279 (H3K27ac, H3K27me3, H3K36me3, H3K4me1, H3K4me3, and H3K9me3)<sup>34,35</sup>. In T<sub>h</sub>17 cells  
280 (**Figure S4A; Supplementary Table 20**), we detected statistically significant enrichments for  
281 H3K27ac (enrichment p-value =  $6.54 \times 10^{-9}$ ), H3K4me1 (p-value =  $3.96 \times 10^{-19}$ ) and H3K4me3 (p-  
282 value =  $2.29 \times 10^{-8}$ ). Similarly, in B cells (**Figure S4B; Supplementary Table 21**), we also  
283 detected significant enrichments for H3K27ac (enrichment p-value =  $1.18 \times 10^{-11}$ ), H3K4me1 (p-  
284 value =  $4.96 \times 10^{-16}$ ) and H3K4me3 (p-value =  $3.93 \times 10^{-8}$ ). These results suggest that MS genetic  
285 association are primarily enriched at active noncoding elements: primed enhancers (H3K4me1),  
286 active enhancers (H3K27ac and H3K4me1) and active promoters (H3K4me3).

287

288 To further delineate the chromatin states with the strongest MS genetic associations, we  
289 examined enrichments of MS GWAS results in the predicted chromatin states for B cells and  
290 T<sub>h</sub>17 T cells as available in the RoadMap Epigenomics Project<sup>36</sup>. For Th17 CD4 T cells, the  
291 “EnhA2” chromatin state (Active Enhancer 2) were statistically enriched (enrichment p-  
292 value= $1.19 \times 10^{-3}$ ) (**Figure S5A; Supplementary Table 22**). For B cells, “Tx3” (Transcribed 3’  
293 preferential; enrichment p-value= $1.80 \times 10^{-3}$ ) and “PromD1” (Promoter Downstream TSS 1; p-  
294 value= $4.40 \times 10^{-4}$ ) were statistically enriched, again reflecting the strongest enrichments at active  
295 regulatory elements (**Figure S5B; Supplementary Table 23**). These results demonstrate that

296 MS GWAS variants act through activating regulatory elements, consistent with the autoimmune  
297 nature of MS.

298

### 299 *Fine-mapping of MS GWAS loci in cell-specific OCRs*

300 We next sought to understand underlying mechanisms by nominating putative causal genes and  
301 variants in a cell-specific fashion. First, we applied statistical fine-mapping to nominate likely  
302 causal SNPs. Most statistical fine-mapping approaches require association information across  
303 all SNPs in a given locus. In contrast, for MS GWAS, genome-wide results are based on  
304 targeted replication analyses, which by design included only a select subset of SNPs within  
305 each locus. To overcome this challenge, we applied PICS to perform statistical fine-mapping,  
306 which as compared to other statistical fine-mapping approaches, does not require GWAS  
307 summary statistics for all SNPs in a region<sup>15</sup>. We defined for each locus a 95% credible set such  
308 that the sum of the posterior probabilities for variants in that credible set is greater than or equal  
309 to 95%. For fine-mapping, we used the joint analysis MS GWAS results, which include only  
310 replicated genome-wide effects<sup>8</sup>. We included all 200 non-MHC loci where the MS GWAS joint  
311 association p-value was less than  $5 \times 10^{-8}$ . Next, we prioritized SNPs if they had a PICS  
312 posterior probability (PP) > 1% and were included in the 95% PICS credible set. This is a liberal  
313 threshold for defining prioritized SNPs, aimed at increasing sensitivity for detecting possible  
314 causal variants. Across the 200 loci, there were 3436 credible set variants (1-58 variants per  
315 locus) (**Figure S6A**). At 19 loci, there was only one variant in the credible set, and at 37 loci,  
316 there were four or fewer prioritized variants (**Figure S6B**).

317

318 Next, we intersected the 3436 credible set variants with OCRs from the 16 hematopoietic cell  
319 populations, which we chose to use as they cover a broad range of hematopoietic cell types<sup>18</sup>.  
320 Across the 200 loci, 870 of the prioritized variants overlapped an OCR in at least one cell type.

321 Remarkably, 163 out of the 200 loci had at least one prioritized variant overlapping an OCR in  
322 any cell type. B and CD4 T cells were the cell types with the greatest number of loci with a  
323 credible set SNP overlapping an OCR, 126 and 125 loci respectively (**Figure S7**).

324

### 325 *Integration of genetic and epigenetic data identifies putative causal genes*

326 The vast majority of GWAS-associated variants are noncoding and regulate genes that may be  
327 far from the variant in terms of linear distance on the genome. To address this challenge and  
328 nominate putative causal genes that are regulated by the MS-associated OCRs, we leveraged  
329 promoter capture Hi-C data (PCHiC), which identifies chromatin looping interactions between  
330 regulatory elements and target gene promoters. We utilized PCHiC data performed on 17  
331 hematopoietic cell populations, which partially overlap with the cell types for which we have  
332 ATAC-seq data<sup>37</sup>. These cell populations include naïve B cells, total B cells, activated CD4 T  
333 cells, non-activated CD4 T cells, and total T cells. We considered only GWAS loci where a  
334 credible set MS GWAS SNP overlapped both an OCR and a PCHiC interaction.

335

336 Through these analyses, we nominated 261 genes within 86 MS loci in B cells and 364 genes  
337 within 115 MS loci in CD4 T cells (**Supplemental Table 24**). We note that these genes are  
338 putative causal genes, representing a list of genes that could be linked with the MS loci via a  
339 regulatory mechanism in the respective cell types. The majority of these genes were shared  
340 between B and CD4 T cells (n=178; 68.2% and 48.9% respectively; **Figure 7A**). We have  
341 previously suggested a list of putative causal genes (n=551) based on an ensemble of methods  
342 that did not include ATAC-seq or chromatin interactions<sup>8</sup>. Of these 551 previously nominated  
343 genes, 67 (12.2%) overlapped with our B cell prioritized genes and 111 (20.1%) with our CD4 T  
344 cell prioritized genes, highlighting that our current mechanism-specific gene prioritization is

345 capturing a large number of potentially causal genes that have not been previously implicated in  
346 MS genetic studies.

347

348 Next, we utilized the list of putative causal genes to identify enriched canonical pathways.

349 Starting with CD4 T and B cell lists, we created additional lists for the common genes (shared  
350 between CD4 T and B cells), and finally genes unique to CD4 T cells and B cells. We observed  
351 widespread pathway enrichment for the putative causal genes of the CD4 T cells (n=294) and B  
352 cells (n=236) at FDR<5%. The common set of genes was enriched in 85 pathways

353 (**Supplemental Table 25**). The B unique gene list (n=83) was enriched in 22 canonical

354 pathways, including lipoprotein and cholesterol pathways, the CD40 pathway, and JAK-STAT

355 pathway (**Figure 7B-C**). The unique genes in CD4 T cells (n=186) were enriched in 99

356 pathways, including TCR pathways, various interleukin pathways, and MAPK/ERK signaling

357 pathways (**Figure 7B-C**).

358

359 Pathway analyses utilize known biological connections for a given set of genes but many of

360 underlying mechanisms could be still uncharacterized. Thus, we leveraged protein-protein

361 interaction (PPI) data to test whether the respective putative causal gene lists exhibit a high

362 degree of connectivity<sup>38</sup>. A similar percent of the mapped CD4 T cell and B cell prioritized genes

363 were directly connected, 48.9% and 43.7% respectively (**Supplementary Table 26; Figures**

364 **S8-12**). Only the CD4 T and CD4 T unique gene lists demonstrated a higher degree of

365 connectivity than expected (p-value<0.05), although all gene lists had communities of genes

366 with high connectivity (p-value<0.05; **Supplementary Table 26**). These results are consistent

367 with the pathway analyses, implying that the MS genetics are mediated by several different

368 mechanisms in both cell types, some of which are shared and some of which are cell-type

369 specific.



370

371 *A fine interplay between shared and cell-specific B and CD4 T cell putative causal genes*

372 The results of the pathways and PPI analyses suggest that the MS genes common and unique  
373 to B and CD4 T cells do not act independently but rather have shared cellular mechanisms. We  
374 illustrate this by studying a locus on chromosome 19 (**Figure 8**) where the lead SNP rs1465697  
375 (chr19:49837246 C>T) has a MS GWAS association p-value of  $3.02 \times 10^{-18}$ . The lead SNP is the  
376 most highly prioritized variant by statistical fine-mapping out of 21 overall SNPs in the 95%  
377 credible set (PP=15% for rs1465697; next highest PP 9%). This SNP overlies an OCR present  
378 in all lymphoid lineages, including B cells, CD4 T cells, and CD8 T cells. We have previously  
379 suggested five putative causal genes for this locus: *DKKL1*, *CCDC155*, *CD37*, *TEAD2*, and  
380 *SLC6A16*<sup>8</sup>. Using PCHiC data, this OCR forms a chromatin loop interaction with *TEAD2* and  
381 *DKKL1*, but not the other three genes. This chromatin loop interaction is observed in activated  
382 CD4 T cells, naïve B cells, total B cells, naïve CD8 T cells, and fetal thymus, but none of the  
383 other hematopoietic cell types<sup>37</sup>. Furthermore, this SNP is an eQTL for *TEAD2* in B cells, but is  
384 not an eQTL for any other gene in this locus in any of the available hematopoietic cell types  
385 (**Figure 8**)<sup>39</sup>. Together, these lines of evidence support *TEAD2* as the causal gene at this locus.

386

387 Interestingly, *TEAD2* is a transcription factor with 1459 predicted regulated genes<sup>40</sup>, including  
388 38 putatively causal CD4 T cell genes and 25 B cell genes as nominated above (FDR < 1 %,  
389 FDR < 1%, respectively; **Figures S13-14**). The majority of these genes are common in both  
390 CD4 T and B cells (n=23; FDR < 1%; **Figure S15**). To identify genes whose expression is  
391 modulated by *TEAD2* in CD4 T and B cells, we examined *TEAD2* knock-down (KD) and over-  
392 expression (OE) in cancer cell lines (n=8, respectively) from the Library of Integrated Network-  
393 Based Cellular Signatures (LINCS) Program<sup>41</sup>. Although these cell lines do not represent an  
394 ideal experimental model to study the effect of *TEAD2* in immune cells, they can still be used to  
395 understand mechanisms reflecting core cellular functions. Within each cell line we identified

396 genes whose expression changed in the opposite direction (top or bottom 10%) in the KD  
397 versus OE models. These ranged from 7 to 24 for the CD4 T cell prioritized genes  
398 (**Supplementary Table 27; Figure S16**) and from 3 to 16 for the B cell genes (**Supplementary**  
399 **Table 28; Figure S17**). Of these, 17 genes and 9 genes changed expression in at least 2 cell  
400 lines, respectively (**Supplementary Tables 27-28**). These data demonstrate that perturbation of  
401 *TEAD2*, a key immune cell transcription factor, results in indirect changes of putative MS causal  
402 genes in B and CD4 T cells.

403

#### 404 **Discussion**

405 In this paper, we integrated MS GWAS with chromatin accessibility data from a broad array of  
406 peripheral immune cells in order to identify putative causal cell types. Our analyses identified  
407 regulatory regions in B cells and CD4 T cells as each being independently enriched for MS  
408 genetics. Within the CD4 T cell and B cell populations, we further identified OCRs from T<sub>H</sub>17  
409 cells and memory B cells as specifically driving their respective enrichments. Chromatin data  
410 from MS patients reiterated these findings and further suggested that immunomodulatory  
411 treatments alter the chromatin accessibility overlying MS-associated GWAS variants. Integration  
412 of PCHiC data led to prioritization of putative causal genes in B and CD4 T cells, identifying  
413 target genes that are both shared and specific to each of these cell populations. The putative  
414 causal genes implicate several known signaling pathways, mostly due to the cell-specific MS-  
415 associated genes, despite these representing a smaller percentage compared to genes shared  
416 between B and CD4 T cells. Finally, we illustrate that the B and CD4 T cells mechanisms are  
417 intertwined by describing how *TEAD2*, a putative causal gene shared between B and CD4 T  
418 cells, contributes to disease susceptibility directly and indirectly by targeting both shared and  
419 cell-specific MS genes.

420

421 Our study provides genetic evidence for the independent involvement of both CD4 T and B cells  
422 in the pathogenesis of MS<sup>1-3</sup>. It further supports the long-debated causal role of memory B  
423 cells in MS<sup>24,42,43</sup>, shown by the highly effective therapies targeting B cell receptors, most  
424 notably ocrelizumab<sup>7</sup>. Through our analyses, we also corroborate decades of research that have  
425 demonstrated a primary role of CD4 T cells in MS, including the importance of T<sub>h</sub>17 T cells  
426<sup>24,44,45</sup>. For both the B cell and T<sub>h</sub>17 T cell populations, we find that active enhancers and  
427 promoters drive the enrichment signal, consistent with activating roles of these cell types in MS  
428 as an autoimmune condition. The complex interplay between the B and CD4 cells in MS  
429 pathogenesis<sup>2,3,42</sup> is also reflected by our finding of some OCRs present in both cell types,  
430 while other OCRs are present only in specific cell populations.

431  
432 Although other peripheral immune cell types have been shown to be involved in MS, including  
433 monocytes, CD8 T cells, and mDCs<sup>24</sup>, we did not identify independent enrichments for these  
434 cell types. One possible explanation for this apparent contradiction is that these cell types might  
435 work secondarily to memory B and T<sub>h</sub>17 cells, which are more directly under influence from MS  
436 GWAS-associated variants. Non-genetic effects, e.g. environment-specific response, could also  
437 explain their role in MS above and beyond any shared mechanisms with B and CD4 T cells.  
438 Further, context-specific studies, such as under various cell activation conditions, would be  
439 necessary to unravel any potential independent influence of these cells by MS genetic variants.  
440 Lastly, while our analyses do not identify an independent genome-wide enrichment for cell types  
441 other than B and CD4 T cells, GWAS variants may still act at individual loci in these other cell  
442 types.

443  
444 One of the key challenges of GWAS is moving from genetic association to biological  
445 mechanisms<sup>10,13,14</sup>. This is driven by three main challenges. First, linkage disequilibrium, while  
446 highly advantageous to discovery of genetic associations, limits our ability to identify the causal

447 variant. Second, as most GWAS variants are noncoding, identifying the gene(s) that are  
448 affected by the causal variant can be difficult. Third, the cell type(s) in which a given associated  
449 variant acts can be unclear. Our study demonstrates how we can use statistical fine-mapping to  
450 help solve the first challenge, though this is not without multiple caveats<sup>46</sup>. We integrated  
451 orthogonal datasets (ATAC-seq, PChIC) to help delineate the likely causal genes and cell types  
452 and overcome the latter two challenges. We document how shared and cell-specific genes  
453 affect putative causal pathways. We further illustrate the complex interplay between shared and  
454 cell-specific putative causal MS genes by studying the *TEAD2* locus, a transcription factor  
455 recently implicated in immune regulation<sup>47</sup>. Together, our study generates important insights into  
456 the driver subpopulations of peripheral immune cells in MS, reinforcing how MS genetics act  
457 primarily through B and CD4 T cells. Our study also demonstrates the need for in-depth context-  
458 specific cellular data to carefully delineate the causal role of each immune cell subset in MS.

459

## 460 **Methods**

### 461 *GWAS summary statistics*

462 We utilized available MS GWAS summary statistics, which included data from 8,278,136  
463 variants across 14,802 individuals with MS (cases) and 26,703 individuals without MS  
464 (controls)<sup>8</sup>. For enrichment analyses, we included only the 6,773,531 variants that were  
465 analyzed in all 15 cohorts of the discovery stage meta-analysis; this resulted in 6,773,531  
466 variants carried forward. We additionally utilized GWAS summary statistics from various  
467 neuropsychiatric disorders or autoimmune disorders: Alzheimer disease (AD)<sup>26</sup>, schizophrenia  
468 (SCZ)<sup>27</sup>, bipolar disorder (BPD)<sup>28</sup>, type 1 diabetes (T1D)<sup>29</sup>, Crohn's disease (CD)<sup>30</sup>, ulcerative  
469 colitis (UC)<sup>30</sup>, systemic lupus erythematosus (SLE)<sup>31</sup>, rheumatoid arthritis (RA)<sup>32</sup>, and primary  
470 biliary cirrhosis (PBC)<sup>33</sup>. All GWAS data were converted to the ".sumstats" format as required by  
471 LDSC using the "munge.py" function in LDSC with default parameters.

472

473 *Epigenetic and eQTL datasets*

474 *Hematopoietic progenitor and terminal ATAC-seq data:* ATAC-seq data for 16 different human  
475 hematopoietic progenitor and terminal populations was obtained from Corces et al.<sup>18</sup> and  
476 Buenrostro et al.<sup>19</sup>. These ATAC-seq profiles were generated on bulk FACS-sorted cells from  
477 human peripheral blood or bone marrow cells. Alignment of the ATAC-seq data and peak-calling  
478 were performed as previously described<sup>20</sup>. To identify cell-type specific peaks for each cell type,  
479 we used ATAC-seq peaks for that cell type and removed any peaks that overlapped with a peak  
480 present in any one of the other 15 cell types. A single base pair overlap was considered to be  
481 overlapping.

482

483 *Immune cell ATAC-seq data:* We used publicly available immune cell ATAC-seq data (NCBI  
484 GEO GSE 118189) derived from flow-sorted peripheral blood cells<sup>21</sup>. As each cell type had  
485 between 1-4 human donors, we merged the raw ATAC-seq data from the individual donors for a  
486 given cell type. We aligned ATAC-seq reads using bowtie2 version 2.2.1<sup>48</sup> with default  
487 parameters and a maximum paired-end insert distance of 2000 base pairs. The bowtie2 index  
488 was constructed with the default parameters for the hg19 reference genome. We filtered out  
489 reads that mapped to the mitochondria and used samtools version 1.10<sup>49</sup> to filter out reads with  
490 MAPQ < 30 and with the flags '- F 1804' and '-f 2'. Additionally, duplicate reads were discarded  
491 using picard version 2.20.6 (<http://broadinstitute.org.github.io/picard>). Finally, chromatin  
492 accessibility peaks were identified with MACS2 version 2.1.1<sup>50</sup> under default parameters and '--  
493 nomodel --nolambda --keep-dup all --call-summits'.

494

495 *ChIP-seq data:* We downloaded available pre-processed ChIP-seq peak calls from ENCODE for  
496 B cells<sup>34</sup>. Where replicates were available, the bed files for the replicates were merged to create  
497 a composite set of peaks for each histone mark. Data for T<sub>H</sub>17 histone ChIP-seq were

498 downloaded from the Roadmap Epigenomics Project<sup>35</sup> (NCBI GEO GSM997225); we used pre-  
499 processed ChIP-seq peak calls generated in Amariuta et al<sup>51</sup>.

500

501 *chromHMM*: We used a 25 chromatin state model<sup>36</sup>, which are imputed based on 12 epigenetic  
502 marks from across 127 epigenomes generated as part of the Roadmap Epigenomics Project<sup>35</sup>.

503 We used the chromatin states from B cells and Th17 CD4+ T cells. Chromatin states were  
504 downloaded from [https://egg2.wustl.edu/roadmap/web\\_portal/chr\\_state\\_learning.html](https://egg2.wustl.edu/roadmap/web_portal/chr_state_learning.html). We  
505 excluded the “Quiescent/Low” cell state, as it encompasses a large proportion of the genome,  
506 resulting in unstable estimates of heritability.

507

508 *Verily ATAC-seq data*: We utilized immune cell ATAC-seq data generated from Verily as part of  
509 the SystemS collaboration with Brigham & Women’s Hospital (PIs: Dr. Chitnis and Dr. Weiner).  
510 Cell sorting: Frozen cryovials in liquid nitrogen were thawed in a 37°C bead bath and centrifuged  
511 for 5 min at 600 x g, 4°C. The cell pellet was washed with 1 mL of FACS buffer, and the wash  
512 repeated. The cell pellet was resuspended in the residual volume with 2.5 uL of 0.33mg/mL S7  
513 DNase. 50 uL of staining cocktail was added for the respective flow cytometry panels to be  
514 analyzed (T cell, B cell, myeloid panel) and incubated for 25 min on ice and in the dark. Cells  
515 were washed in FACS buffer, resuspended in a final volume of 400 uL FACS buffer, and passed  
516 through a 35 µm cell strainer cap. Stained samples were sorted on a FACSAria Fusion (BD  
517 Biosciences, San Jose, CA). Using FACSDiva v8.0.1 software, the samples were gated first by  
518 forward and side scatter properties, then FSC-H vs FSC-A for singlet discrimination, and finally,  
519 with their respective markers for each cell type (**Supplementary Table 29**). For each cell type  
520 of interest, up to 500 cells were sorted into the tagmentation buffer.

521 ATAC-seq library preparation and sequencing: Cells were sorted directly into 20 uL of cold  
522 tagmentation buffer (10 uL TD, 2 uL 2% IGEPAL CA-630, 6 uL nuclease-free H<sub>2</sub>O, 2 uL TDE1  
523 per sample), followed by incubation at 37°C for 30 min with shaking at 500 RPM. Samples were

524 stored at -20°C until further processing. DNA was extracted with the QIAGEN MinElute PCR  
525 purification kit according to the manufacturer's protocol, and samples were amplified with KAPA  
526 HiFi kits and Illumina Nextera indices. The amplified material was cleaned with the QIAGEN  
527 MinElute PCR purification kit and quantified using KAPA library quantification kits. Samples  
528 were normalized and pooled for sequencing on the NextSeq (Illumina).  
529 Processing: Paired-end raw ATAC-seq reads were trimmed using NGmerge<sup>60</sup> using the default  
530 parameters. The reads were then aligned to GRCh38 using Bowtie2 version 2.3.5<sup>49</sup>. The  
531 resulting SAM files were converted and sorted into BAM format using samtools version 1.5<sup>50</sup>.  
532 We filtered out the reads with MAPQ<10 and reads that were aligned to mitochondria using  
533 samtools. In addition, duplicate reads were removed using picard version 2.20.6  
534 (<http://broadinstitute.org.github.io/picard>). Finally, peaks were called using MACS2 version 2.2.5  
535<sup>51</sup> with default parameters and --keep-dup all --nomodel --nolambda. To obtain peaks for each  
536 cell type, we merged the peak files from all samples for that specific cell type using bedtools  
537 version 2.29<sup>61</sup>.

538

### 539 *Enrichment of GWAS results within ATAC-seq peaks*

540 To calculate enrichments of the MS GWAS data within annotations (e.g., ATAC-seq or CHIP-  
541 seq peaks), we applied stratified LD Score regression (LDSC)<sup>16,23</sup>. LDSC was performed using  
542 LDSC v1.0.0 (<https://github.com/bulik/LDSC>), which was run on the discovery summary  
543 statistics from the MS GWAS discovery stage summary statistics<sup>8</sup>. The human MHC locus was  
544 excluded given its complex LD patterns as recommended by Finucane et al.<sup>16</sup>  
545 To run LDSC, we used precomputed LD scores based on the European ancestry samples of the  
546 1000 Genomes Project Phase 1<sup>52</sup> which was restricted to HapMap3 SNPs<sup>53</sup>, and we generated  
547 partitioned LD scores for each set of annotations. To perform LDSC, we regressed the summary  
548 statistics ( $\chi^2$ ) from a given GWAS on to annotation-specific LD scores, with baseline scores

549 (original 53 annotation model), regression weights and allele frequencies based on 1000  
550 Genome Project Phase 1 data as precomputed by software authors. We applied partitioned  
551 heritability analyses using LDSC under three different models:

- 552 1) To ask how much a given annotation contributes to trait heritability, we used a LDSC  
553 model that includes baseline annotations and an annotation of interest. The heritability  
554 enrichment of the annotation was defined as the proportion of SNP heritability in the  
555 category divided by the proportion of SNPs in that category; we report statistical  
556 significance of this enrichment as p-values.
- 557 2) When comparing multiple annotations (e.g., ATAC-seq peaks from different cell types),  
558 we ran a LDSC model that includes the baseline model and annotations from all cell  
559 types. In this scenario, we calculate for each annotation the coefficient  $\tau_c$  which  
560 measures the contribution to SNP heritability for a given annotation to heritability in this  
561 overall model, stratified on other annotations in the model. Z-scores for the coefficient  $\tau_c$   
562 were converted to a one-sided p-value, which we report as a measure of statistical  
563 significance.
- 564 3) We also performed LDSC on pairs of annotations, which we term pairwise stratified  
565 LDSC. In these models, we include the baseline model, an index annotation of interest,  
566 and a comparator annotation of interest. To run LDSC, we used a previously described  
567 extension of LDSC <sup>54</sup>.

568 Throughout, all default LDSC parameters were used.

569

### 570 *Statistical fine-mapping*

571 Statistical fine-mapping was performed using the marginal p-values from the replication (joint  
572 analysis) summary statistics from the MS GWAS <sup>8</sup>. The 200 genome-wide significant loci at  
573  $p < 5 \times 10^{-8}$  were used. LD was calculated between each lead variant and all variants with  $r^2 > 0.2$   
574 and within a 2 Mb window based on the 1000 Genomes Phase 1 (European subset) reference



575 panel<sup>52</sup>. PLINK v1.90b3.32 was used to perform LD calculations<sup>55,56</sup> with parameters of ‘--r2 --ld-  
576 window-kb 2000 --ld-window 999999 --ld-window-r2 0.2’.

577

578 We then applied PICS to each locus<sup>15</sup>. Briefly, PICS uses the lead association p-value and LD  
579 structure of the locus to calculate the most likely causal SNPs given the observed lead  
580 association signal. PICS probabilities represent the probability of a given SNP in a locus being  
581 the causal SNP. Default PICS parameters were used. From the PICS probabilities, we  
582 calculated 95% credible sets (CS). We defined the 95% CS as a set of variants such that the  
583 true causal variant has a 95% chance of being in the credible set. To calculate credible sets, for  
584 each locus, we ranked variants in descending order by their PICS probabilities. We then  
585 iteratively added variants to the credible set for that locus until the sum of their PICS  
586 probabilities was greater than or equal to 0.95. For CS inclusion, we also required the variant to  
587 have a PICS probability > 0.1.

588

### 589 *Identification of target genes*

590 We leveraged promoter capture Hi-C (PCHiC) data from 17 hematopoietic cell populations to  
591 link genetic associations with genes that they may regulate<sup>37</sup>. We filtered the PCHiC dataset for  
592 looping interactions with a CHiCAGO score > 5<sup>57</sup>. An overlap between a GWAS variant and a  
593 PCHiC looping interaction was considered if the GWAS variant overlapped any position in the  
594 non-promoter (“other end”) of the PCHiC interaction. For CD4<sup>+</sup> T cells, we considered only  
595 GWAS SNPs that overlapped an ATAC-seq peak in bulk CD4<sup>+</sup> T cells or any of the CD4<sup>+</sup> T cell  
596 subsets (naïve effector CD4<sup>+</sup> T cells, T<sub>h</sub>1, T<sub>h</sub>2, T<sub>h</sub>17, follicular T<sub>h</sub>, naïve T<sub>regs</sub> and memory T<sub>regs</sub>),  
597 and which overlapped a PCHiC interaction in naïve CD4<sup>+</sup> T cells (nCD4), total CD4<sup>+</sup> T cells  
598 (tCD4), non-activated total CD4<sup>+</sup> T cells (naCD4), or activated total CD4<sup>+</sup> T cells (aCD4). For B  
599 cells, we considered only GWAS SNPs that overlapped an ATAC-seq peak in bulk B cells or

600 any of the B cell subsets (naïve B cells, memory B cells, or plasmablasts), and which  
601 overlapped a PCHiC interaction in naïve B cells (nB) or total B cells (tB).

602

### 603 *Correction for multiple hypothesis testing*

604 Throughout our manuscript, we use Bonferroni corrections when testing multiple hypotheses. To  
605 generate a Bonferroni-corrected p-value threshold, we used a traditional p-value threshold of  
606 0.05 divided by the number of tests being performed in a given analysis. We note that as many  
607 of the tests are correlated (since the underlying annotations are often highly correlated with  
608 each other), the effective number of independent tests being performed is fewer than the  
609 number of tests actually performed. As such, our analyses are overly conservative. We decided  
610 on this approach of using Bonferroni corrections as opposed to false discovery rate (FDR)  
611 approaches, as the number of tests being performed is often small, leading to unstable  
612 estimates of FDR.

613

### 614 *Gene set enrichment analyses*

615 We performed pathway analyses utilizing the canonical pathways (CP) of the Molecular  
616 Signatures Database (MSigDB v7.2), as it is available from the Gene Set  
617 Enrichment Analysis website (<http://software.broadinstitute.org/gsea/msigdb>). We  
618 ran the Canonical Pathways, Biocarta, KEGG, and Reactome gene sets categories  
619 together in the same model. We estimated statistical significance using the hypergeometric  
620 distribution and applied false discovery correction, as previously described<sup>8</sup>. The same model  
621 was applied for the enrichment of prioritized gene sets with Gene Transcription Regulation  
622 Database (GTRD) transcription factor targets gene sets<sup>40</sup>. Significant enrichment level was set  
623 to a false discovery rate < 5%.

624

### 625 *Protein-protein interaction networks*

626 We utilized GeNets (<https://apps.broadinstitute.org/genets>)<sup>38</sup> to leverage known protein-protein  
627 interactions (PPI) of our prioritized gene sets. GeNets uses a random forest  
628 classified, trained in PPI data with 18 parameters that capture information about  
629 centrality and clustering. It creates communities of genes, sets of genes (nodes) that are  
630 connected to each other more than genes outside this community. Furthermore, it uses the  
631 random forest classifier and the connectivity to the tested gene set to propose candidate  
632 genes. For each described network the p-value is estimated by testing whether the number  
633 of observed edges divided by the numbers of possible edges using permutations. We ran  
634 GeNets via the web interface with the GeNets Metanetwork v1.0 and utilizing the InWeb model  
635 (“Override network the analysis model was trained on” option).

636

#### 637 *TEAD2 knockdown and over-expression in LINCS cell lines*

638 Robust z-scores, “level 5 data”, from knock-down (KD) or over-expression (OE) of *TEAD2* in  
639 cancer cell lines<sup>41</sup> were downloaded from clue.io  
640 (<https://clue.io/command?q=/sig%20%22TEAD2%22>). The robust z scores represent differential  
641 expression for each genetic perturbation, adjusted for the gene expression of all other  
642 perturbations on the same physical plate. For knockdown and over-expression experiments the  
643 differential expression comparator were samples using a vector control, which are negative  
644 genetic controls that either lack a gene-specific sequence or target a non-human gene (like  
645 GFP).

646

647 **Data availability**

648 MS GWAS summary statistics are available via request to the IMSGC (<https://imsgc.net/>). LD  
649 score regression software and reference panels were obtained from software developers  
650 (<https://github.com/bulik/LDSC>). Processed GWAS summary statistics for diseases other than  
651 MS were obtained from [https://alkesgroup.broadinstitute.org/LDSCORE/independent\\_sumstats/](https://alkesgroup.broadinstitute.org/LDSCORE/independent_sumstats/).  
652 1000 Genomes Phase 1 reference panel was obtained from  
653 <ftp://ftp.1000genomes.ebi.ac.uk/vol1/ftp/>. Hematopoietic ATAC-seq data for Buenrostro et al  
654 was obtained from NCBI GEO (accession GSE74912). Hematopoietic ATAC-seq data from  
655 Calderon et al was obtained from NCBI GEO (accession GSE118189). CHIP-seq data from  
656 Roadmap were obtained from NCBI GEO (accession GSM997225). chromHMM chromatin state  
657 partitions for ENCODE were obtained from  
658 [https://egg2.wustl.edu/roadmap/web\\_portal/chr\\_state\\_learning.html](https://egg2.wustl.edu/roadmap/web_portal/chr_state_learning.html). PChIC data were  
659 downloaded from Data S1 in the referenced manuscript  
660 (<https://www.sciencedirect.com/science/article/pii/S0092867416313228>). DICE eQTL data were  
661 obtained from <https://dice-database.org/>.  
662 The Verily Life Sciences ATAC-seq from the SystemS data can be requested by Charlie Kim  
663 ([charliekim@verily.com](mailto:charliekim@verily.com)).  
664 The LINCS KD and OE TEAD2 data can be accessed through the Broad Connectivity Map  
665 portal at clue.io: <https://clue.io/command?q=/sig%20%22TEAD2%22>.

666

667 **References**

- 668 1. Filippi M, Bar-Or A, Piehl F, et al. Multiple sclerosis. *Nat Rev Dis Prim*. 2018;4(1):43.  
669 doi:10.1038/s41572-018-0041-4
- 670 2. Baecher-Allan C, Kaskow BJ, Weiner HL. Multiple Sclerosis: Mechanisms and  
671 Immunotherapy. *Neuron*. 2018;97(4):742-768. doi:10.1016/j.neuron.2018.01.021
- 672 3. van Langelaar J, Rijvers L, Smolders J, van Luijn MM. B and T Cells Driving Multiple  
673 Sclerosis: Identity, Mechanisms and Potential Triggers. *Front Immunol*. 2020;11:760.  
674 doi:10.3389/fimmu.2020.00760
- 675 4. Chihara N. Dysregulated T cells in multiple sclerosis. *Clin Exp Neuroimmunol*. 2018;9:20-  
676 29. doi:10.1111/cen3.12438
- 677 5. Negron A, Robinson RR, Stüve O, Forsthuber TG. The role of B cells in multiple  
678 sclerosis: Current and future therapies. *Cell Immunol*. 2019;339:10-23.  
679 doi:10.1016/j.cellimm.2018.10.006
- 680 6. Greenfield AL, Hauser SL. B-cell Therapy for Multiple Sclerosis: Entering an era. *Ann*  
681 *Neurol*. 2018;83(1):13-26. doi:10.1002/ana.25119
- 682 7. Hauser SL, Bar-Or A, Comi G, et al. Ocrelizumab versus Interferon Beta-1a in Relapsing  
683 Multiple Sclerosis. *N Engl J Med*. 2017;376(3):221-234. doi:10.1056/NEJMoa1601277
- 684 8. Patsopoulos NA, Baranzini SE, Santaniello A, et al. Multiple sclerosis genomic map  
685 implicates peripheral immune cells and microglia in susceptibility. *Science (80- )*. 2019.  
686 doi:10.1126/science.aav7188
- 687 9. Consortium IMSG. Low-Frequency and Rare-Coding Variation Contributes to Multiple  
688 Sclerosis Risk. *Cell*. 2018;175(6):1679-1687.e7. doi:10.1016/j.cell.2018.09.049
- 689 10. Visscher PM, Wray NR, Zhang Q, et al. 10 Years of GWAS Discovery: Biology, Function,  
690 and Translation. *Am J Hum Genet*. 2017;101(1):5-22. doi:10.1016/j.ajhg.2017.06.005
- 691 11. Gusev A, Lee SH, Trynka G, et al. Partitioning heritability of regulatory and cell-type-  
692 specific variants across 11 common diseases. *Am J Hum Genet*. 2014;95(5):535-552.

- 693 doi:10.1016/j.ajhg.2014.10.004
- 694 12. Cano-Gamez E, Trynka G. From GWAS to Function: Using Functional Genomics to  
695 Identify the Mechanisms Underlying Complex Diseases. *Front Genet.* 2020;11:424.  
696 doi:10.3389/fgene.2020.00424
- 697 13. Edwards SL, Beesley J, French JD, Dunning AM. Beyond GWASs: Illuminating the Dark  
698 Road from Association to Function. *Am J Hum Genet.* 2013;93(5):779-797.  
699 doi:10.1016/j.ajhg.2013.10.012
- 700 14. Gallagher MD, Chen-Plotkin AS. The Post-GWAS Era: From Association to Function. *Am*  
701 *J Hum Genet.* 2018;102(5):717-730. doi:10.1016/j.ajhg.2018.04.002
- 702 15. Farh KK-H, Marson A, Zhu J, et al. Genetic and epigenetic fine mapping of causal  
703 autoimmune disease variants. *Nature.* 2015;518(7539):337-343.  
704 doi:10.1038/nature13835
- 705 16. Finucane HK, Bulik-Sullivan B, Gusev A, et al. Partitioning heritability by functional  
706 annotation using genome-wide association summary statistics. *Nat Genet.*  
707 2015;47(11):1228-1235. doi:10.1038/ng.3404
- 708 17. International Multiple Sclerosis Genetics Consortium. A systems biology approach  
709 uncovers cell-specific gene regulatory effects of genetic associations in multiple sclerosis.  
710 *Nat Commun.* 2019;10(1):2236. doi:10.1038/s41467-019-09773-y
- 711 18. Corces MR, Buenrostro JD, Wu B, et al. Lineage-specific and single-cell chromatin  
712 accessibility charts human hematopoiesis and leukemia evolution. *Nat Genet.*  
713 2016;48(10):1193-1203. doi:10.1038/ng.3646
- 714 19. Buenrostro JD, Corces MR, Lareau CA, et al. Integrated Single-Cell Analysis Maps the  
715 Continuous Regulatory Landscape of Human Hematopoietic Differentiation. *Cell.*  
716 2018;173(6):1535-1548.e16. doi:10.1016/j.cell.2018.03.074
- 717 20. Ulirsch JC, Lareau CA, Bao EL, et al. Interrogation of human hematopoiesis at single-cell  
718 and single-variant resolution. *Nat Genet.* 2019;51(4):683-693. doi:10.1038/s41588-019-

- 719 0362-6
- 720 21. Calderon D, Nguyen MLT, Mezger A, et al. Landscape of stimulation-responsive  
721 chromatin across diverse human immune cells. *Nat Genet.* 2019. doi:10.1038/s41588-  
722 019-0505-9
- 723 22. Finucane HK, Bulik-Sullivan B, Gusev A, et al. Partitioning heritability by functional  
724 annotation using genome-wide association summary statistics. *Nat Genet.*  
725 2015;47(11):1228-1235. doi:10.1038/ng.3404
- 726 23. Bulik-Sullivan BK, Loh P-R, Finucane HK, et al. LD Score regression distinguishes  
727 confounding from polygenicity in genome-wide association studies. *Nat Genet.*  
728 2015;47(3):291-295. doi:10.1038/ng.3211
- 729 24. Dendrou CA, Fugger L, Friese MA. Immunopathology of multiple sclerosis. *Nat Rev*  
730 *Immunol.* 2015;15(9):545-558. doi:10.1038/nri3871
- 731 25. Fani Maleki A, Rivest S. Innate Immune Cells: Monocytes, Monocyte-Derived  
732 Macrophages and Microglia as Therapeutic Targets for Alzheimer's Disease and Multiple  
733 Sclerosis. *Front Cell Neurosci.* 2019;13. doi:10.3389/fncel.2019.00355
- 734 26. Lambert JC, Ibrahim-Verbaas CA, Harold D, et al. Meta-analysis of 74,046 individuals  
735 identifies 11 new susceptibility loci for Alzheimer's disease. *Nat Genet.*  
736 2013;45(12):1452-1458. doi:10.1038/ng.2802
- 737 27. Schizophrenia Working Group of the Psychiatric Genomics Consortium. Biological  
738 insights from 108 schizophrenia-associated genetic loci. *Nature.* 2014;511(7510):421-  
739 427. doi:10.1038/nature13595
- 740 28. Psychiatric GWAS Consortium Bipolar Disorder Working Group. Large-scale genome-  
741 wide association analysis of bipolar disorder identifies a new susceptibility locus near  
742 ODZ4. *Nat Genet.* 2011;43(10):977-983. doi:10.1038/ng.943
- 743 29. Bradfield JP, Qu H-Q, Wang K, et al. A genome-wide meta-analysis of six type 1 diabetes  
744 cohorts identifies multiple associated loci. McCarthy MI, ed. *PLoS Genet.*

- 745 2011;7(9):e1002293. doi:10.1371/journal.pgen.1002293
- 746 30. Jostins L, Ripke S, Weersma RK, et al. Host-microbe interactions have shaped the  
747 genetic architecture of inflammatory bowel disease. *Nature*. 2012;491(7422):119-124.  
748 doi:10.1038/nature11582
- 749 31. Bentham J, Morris DL, Graham DSC, et al. Genetic association analyses implicate  
750 aberrant regulation of innate and adaptive immunity genes in the pathogenesis of  
751 systemic lupus erythematosus. *Nat Genet*. 2015;47(12):1457-1464. doi:10.1038/ng.3434
- 752 32. Okada Y, Wu D, Trynka G, et al. Genetics of rheumatoid arthritis contributes to biology  
753 and drug discovery. *Nature*. 2014;506(7488):376-381. doi:10.1038/nature12873
- 754 33. Cordell HJ, Han Y, Mells GF, et al. International genome-wide meta-analysis identifies  
755 new primary biliary cirrhosis risk loci and targetable pathogenic pathways. *Nat Commun*.  
756 2015;6(1):8019. doi:10.1038/ncomms9019
- 757 34. Bernstein BE, Birney E, Dunham I, Green ED, Gunter C, Snyder M. An integrated  
758 encyclopedia of DNA elements in the human genome. *Nature*. 2012;489:57-74.  
759 doi:10.1038/nature11247
- 760 35. Consortium RE, Kundaje A, Meuleman W, et al. Integrative analysis of 111 reference  
761 human epigenomes. *Nature*. 2015;518(7539):317-330. doi:10.1038/nature14248
- 762 36. Ernst J, Kellis M. Chromatin-state discovery and genome annotation with ChromHMM.  
763 *Nat Protoc*. 2017. doi:10.1038/nprot.2017.124
- 764 37. Javierre BM, Burren OS, Wilder SP, et al. Lineage-Specific Genome Architecture Links  
765 Enhancers and Non-coding Disease Variants to Target Gene Promoters. *Cell*.  
766 2016;167(5):1369-1384.e19. doi:10.1016/j.cell.2016.09.037
- 767 38. Li T, Kim A, Rosenbluh J, et al. GeNets: A unified web platform for network-based  
768 genomic analyses. *Nat Methods*. 2018;15(7):543-546. doi:10.1038/s41592-018-0039-6
- 769 39. Schmiedel BJ, Singh D, Madrigal A, et al. Impact of Genetic Polymorphisms on Human  
770 Immune Cell Gene Expression. *Cell*. 2018;175(6):1701-1715.e16.



- 771 doi:10.1016/j.cell.2018.10.022
- 772 40. Yevshin I, Sharipov R, Kolmykov S, Kondrakhin Y, Kolpakov F. GTRD: A database on  
773 gene transcription regulation - 2019 update. *Nucleic Acids Res.* 2019.  
774 doi:10.1093/nar/gky1128
- 775 41. Subramanian A, Narayan R, Corsello SM, et al. A Next Generation Connectivity Map:  
776 L1000 Platform and the First 1,000,000 Profiles. *Cell.* 2017.  
777 doi:10.1016/j.cell.2017.10.049
- 778 42. Jelcic I, Al Nimer F, Wang J, et al. Memory B Cells Activate Brain-Homing, Autoreactive  
779 CD4+ T Cells in Multiple Sclerosis. *Cell.* 2018;175(1):85-100.e23.  
780 doi:10.1016/j.cell.2018.08.011
- 781 43. Li R, Rezk A, Miyazaki Y, et al. Proinflammatory GM-CSF-producing B cells in multiple  
782 sclerosis and B cell depletion therapy. *Sci Transl Med.* 2015;7(310):310ra166.  
783 doi:10.1126/scitranslmed.aab4176
- 784 44. Kebir H, Ifergan I, Alvarez JI, et al. Preferential recruitment of interferon- $\gamma$ -expressing T<sub>H</sub>  
785 17 cells in multiple sclerosis. *Ann Neurol.* 2009;66(3):390-402. doi:10.1002/ana.21748
- 786 45. Kebir H, Kreymborg K, Ifergan I, et al. Human TH17 lymphocytes promote blood-brain  
787 barrier disruption and central nervous system inflammation. *Nat Med.* 2007;13(10):1173-  
788 1175. doi:10.1038/nm1651
- 789 46. Benner C, Havulinna AS, Järvelin M-R, Salomaa V, Ripatti S, Pirinen M. Prospects of  
790 Fine-Mapping Trait-Associated Genomic Regions by Using Summary Statistics from  
791 Genome-wide Association Studies. *Am J Hum Genet.* 2017;101(4):539-551.  
792 doi:10.1016/j.ajhg.2017.08.012
- 793 47. Bai X, Huang L, Niu L, et al. Mst1 positively regulates B-cell receptor signaling via CD19  
794 transcriptional levels. *Blood Adv.* 2016;1(3):219-230.  
795 doi:10.1182/bloodadvances.2016000588
- 796 48. Langmead B, Salzberg SL. Fast gapped-read alignment with Bowtie 2. *Nat Methods.*

- 797 2012;9(4):357-359. doi:10.1038/nmeth.1923
- 798 49. Li H, Handsaker B, Wysoker A, et al. The Sequence Alignment/Map format and  
799 SAMtools. *Bioinformatics*. 2009;25(16):2078-2079. doi:10.1093/bioinformatics/btp352
- 800 50. Zhang Y, Liu T, Meyer CA, et al. Model-based analysis of ChIP-Seq (MACS). *Genome*  
801 *Biol*. 2008;9(9):R137. doi:10.1186/gb-2008-9-9-r137
- 802 51. Amariuta T, Luo Y, Gazal S, et al. IMPACT: Genomic Annotation of Cell-State-Specific  
803 Regulatory Elements Inferred from the Epigenome of Bound Transcription Factors. *Am J*  
804 *Hum Genet*. 2019;104(5):879-895. doi:10.1016/j.ajhg.2019.03.012
- 805 52. 1000 Genomes Project Consortium, Abecasis GR, Auton A, et al. An integrated map of  
806 genetic variation from 1,092 human genomes. *Nature*. 2012;491(7422):56-65.  
807 doi:10.1038/nature11632
- 808 53. Altshuler DM, Gibbs RA, Peltonen L, et al. Integrating common and rare genetic variation  
809 in diverse human populations. *Nature*. 2010;467(7311):52-58. doi:10.1038/nature09298
- 810 54. Finucane HK, Reshef YA, Anttila V, et al. Heritability enrichment of specifically expressed  
811 genes identifies disease-relevant tissues and cell types. *Nat Genet*. 2018;50(4):621-629.  
812 doi:10.1038/s41588-018-0081-4
- 813 55. Chang CC, Chow CC, Tellier LC, Vattikuti S, Purcell SM, Lee JJ. Second-generation  
814 PLINK: rising to the challenge of larger and richer datasets. *Gigascience*. 2015;4(1):7.  
815 doi:10.1186/s13742-015-0047-8
- 816 56. Purcell S, Neale B, Todd-Brown K, et al. PLINK: a tool set for whole-genome association  
817 and population-based linkage analyses. *Am J Hum Genet*. 2007;81(3):559-575.  
818 doi:10.1086/519795
- 819 57. Cairns J, Freire-Pritchett P, Wingett SW, et al. CHiCAGO: robust detection of DNA  
820 looping interactions in Capture Hi-C data. *Genome Biol*. 2016;17(1):127.  
821 doi:10.1186/s13059-016-0992-2
- 822

823 ***Acknowledgements***

824 NAP was supported in part by National Multiple Sclerosis Society (grants  
825 JF-1808-32223 and RG-1707-28657). This work was supported in part by the Water Cove  
826 Charitable Foundation. We thank Jacob Ulirsch for technical assistance with the use of LD  
827 score regression.

828

829 ***Author contributions.***

830 MHG and NAP had the original idea and supervised the project. JB, CC, XD, PK, CCK, TO, TS,  
831 and DZS generated data. HLW and TC provided samples. MHG, PS, BAL, HL, and NAP  
832 performed analyses. MHG and NAP wrote a first draft of the paper. All authors reviewed results,  
833 contributed to writing and final approval of the paper.

834 ***Competing interests.***

835 JB, CC, XD, PK, CCK, TO, TS, and DZS employment in Verily Life Sciences at time of study.

836

837 ***Correspondence.***

838 Correspondence should be addressed to Nikolaos Patsopoulos  
839 ([npatsopoulos@rics.bwh.harvard.edu](mailto:npatsopoulos@rics.bwh.harvard.edu)) and Michael Guo  
840 ([michael.guo@pennmedicine.upenn.edu](mailto:michael.guo@pennmedicine.upenn.edu))

841

842 ***Computer code***

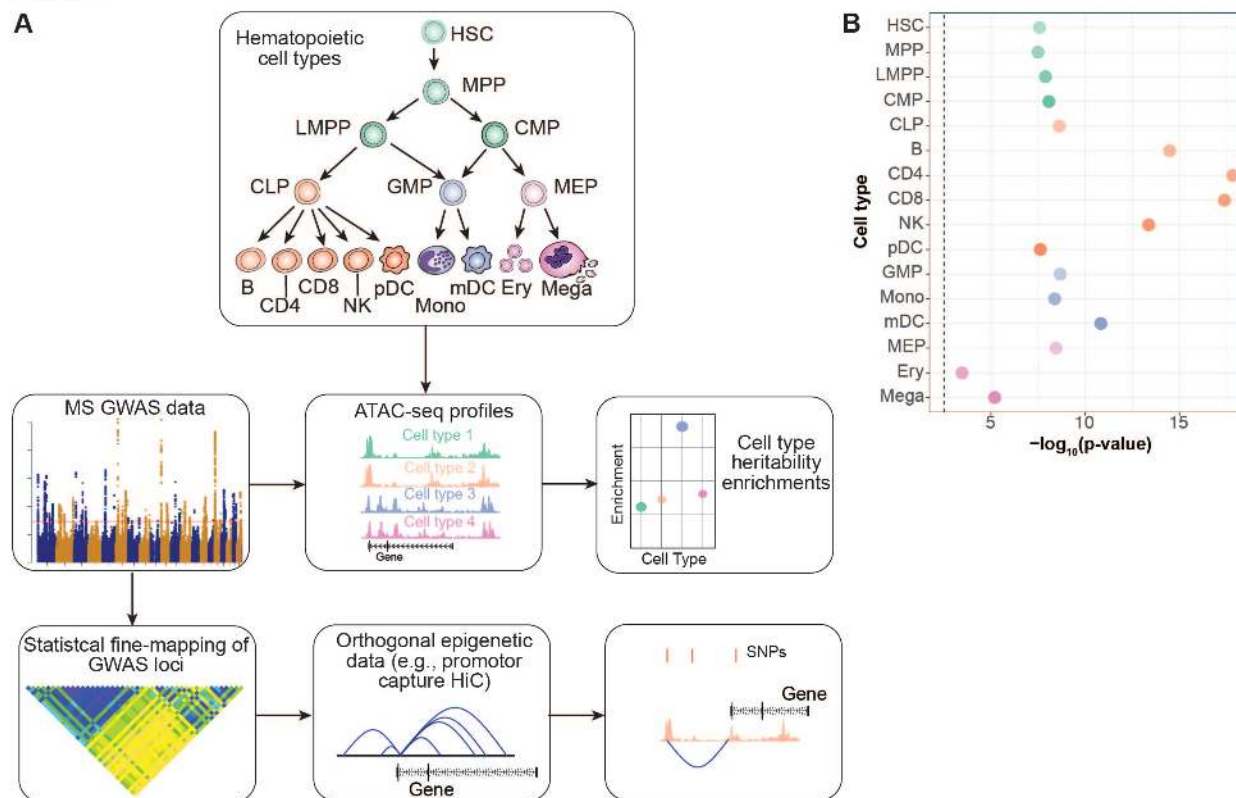
843 Code used in this paper can be accessed in bitbucket:

844 [https://bitbucket.org/patslab/pis\\_ms\\_enrichment/](https://bitbucket.org/patslab/pis_ms_enrichment/)

845 **Figures**

846 **Figure 1: A:** Experimental Design. Top box shows the hematopoietic cell types analyzed. MS  
 847 discovery GWAS results were integrated with ATAC-seq profiles generated from the  
 848 hematopoietic cell types. LDSC was performed to evaluate enrichment of MS GWAS in the  
 849 OCRs of each hematopoietic cell type. Statistical fine-mapping was also performed on the MS  
 850 GWAS results, which were then integrated with orthogonal epigenetic data such as promotor  
 851 capture HiC interactions. This integration of fine-mapping and epigenetic data allowed for  
 852 identification of putative causal mechanisms at individual loci. **B:** Enrichment of MS GWAS  
 853 heritability in hematopoietic cell OCRs. Enrichment p-values are shown as  $-\log_{10}(\text{p-value})$ .

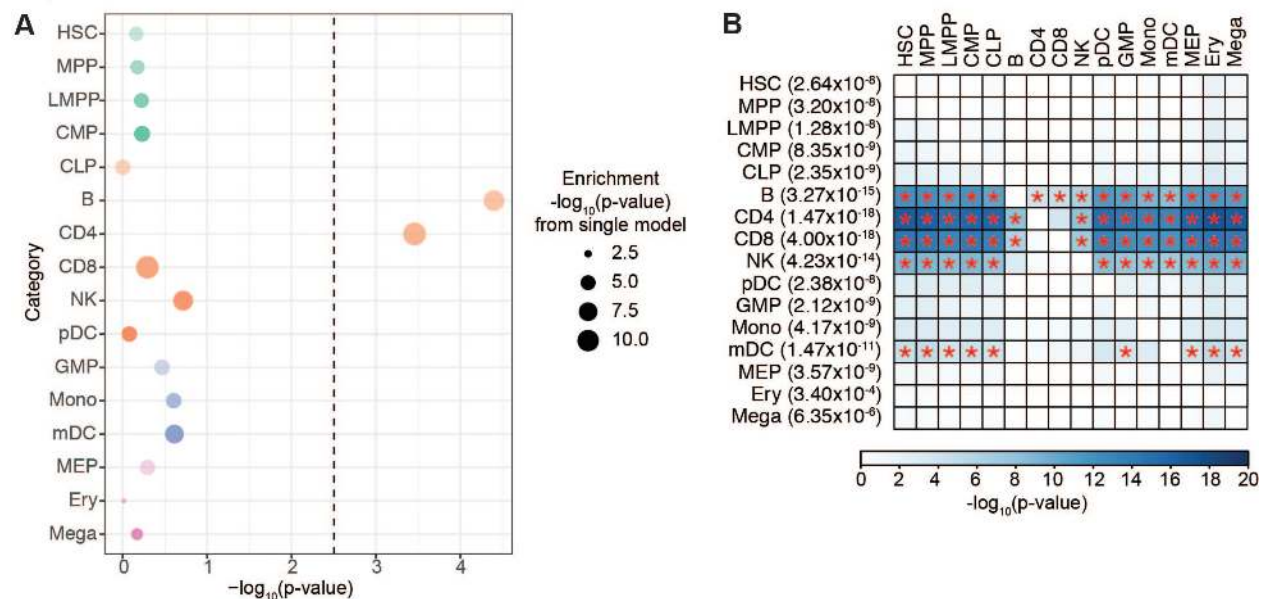
**Figure 1**



854  
 855 **Figure 2: A:** LDSC enrichment results for MS GWAS enrichment in OCRs from across  
 856 hematopoietic cell types in a joint model. Heights of the circles reflect LDSC coefficient ( $\tau_c$ ) p-  
 857 values, which measures whether the annotation (i.e., OCRs for a given cell type) contributes  
 858 significantly to SNP heritability in an overall model that includes OCRs for all hematopoietic cell

859 types and baseline annotations. Sizes of the circles are proportional to the enrichment p-values  
 860 for that given cell type, with larger circles reflecting more significant p-values. **B**: LDSC  
 861 enrichment p-values for pairwise stratified LDSC of MS GWAS results in OCRs from  
 862 hematopoietic cell types. Y-axis are the index cell types with LDSC enrichment p-values prior to  
 863 stratifying in parentheses. X-axis shows the comparator cell type being conditioned upon. Boxes  
 864 are shaded by the LDSC coefficient p-values for the index cell type after conditioning on the  
 865 comparator cell type in the pairwise model (with darker colors representing stronger  
 866 enrichments). Red stars indicate pair-wise comparisons that are statistical significant a  
 867 Bonferroni corrected p-value threshold of  $2.2 \times 10^{-4}$ .

**Figure 2**

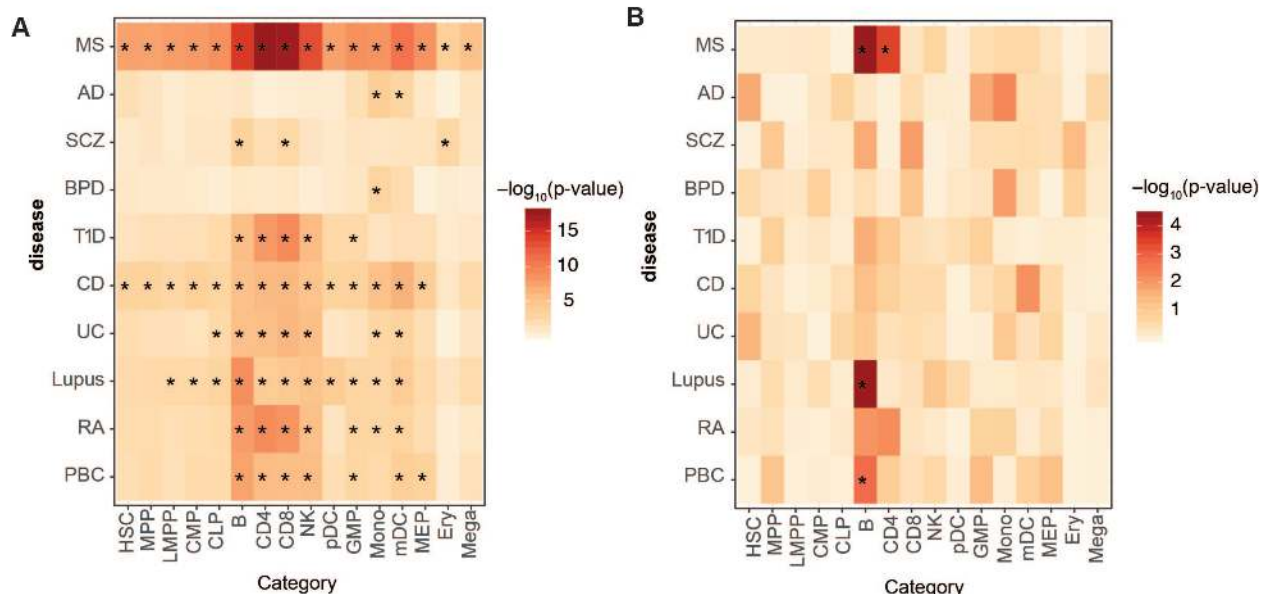


868

869

870 **Figure 3: A**: Enrichments of GWAS results from 10 neuropsychiatric or autoimmune conditions  
 871 in OCRs across various hematopoietic cell types. **B**: LDSC coefficient p-values in the joint  
 872 model across hematopoietic cell ATAC-seq in 10 neuropsychiatric or autoimmune conditions.  
 873 For **A** and **B**, boxes are shaded by  $-\log_{10}(\text{p-value})$ , with darker shading reflecting more  
 874 statistical significance, and statistically significant p-values ( $\text{p-values} < 3.13 \times 10^{-3}$ ) are starred.

Figure 3



875

876

877 **Figure 4: A:** Schematic of lineage relationships among CD4<sup>+</sup> T cell subsets for which ATAC-seq

878 data was analyzed. **B:** LDSC heritability enrichment p-values for CD4<sup>+</sup> T cell subsets in MS

879 GWAS. See Figure 1B for additional description. **C:** LDSC coefficient p-values for CD4<sup>+</sup> T cells

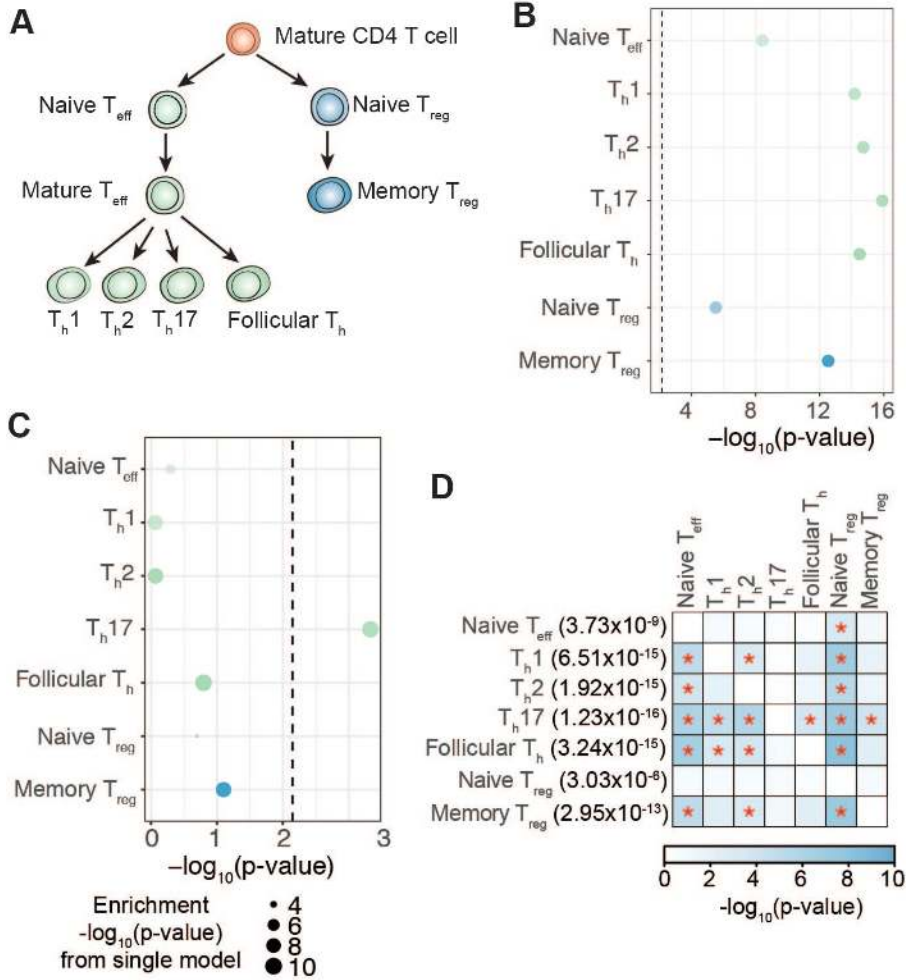
880 in MS GWAS. See Figure 2A for additional description. **D:** LDSC coefficient p-values for

881 pairwise stratified analyses of MS GWAS results in ATAC-seq data from CD4<sup>+</sup> T cell subsets.

882 See Figure 2B legend for additional desc



**Figure 4**



883

884 ription.

885

886

887 **Figure 5: A:** Schematic of lineage relationships among B cell lineage cell types for which ATAC-

888 seq data was analyzed. **B:** LDSC heritability enrichment p-values for B cell lineage cell types in

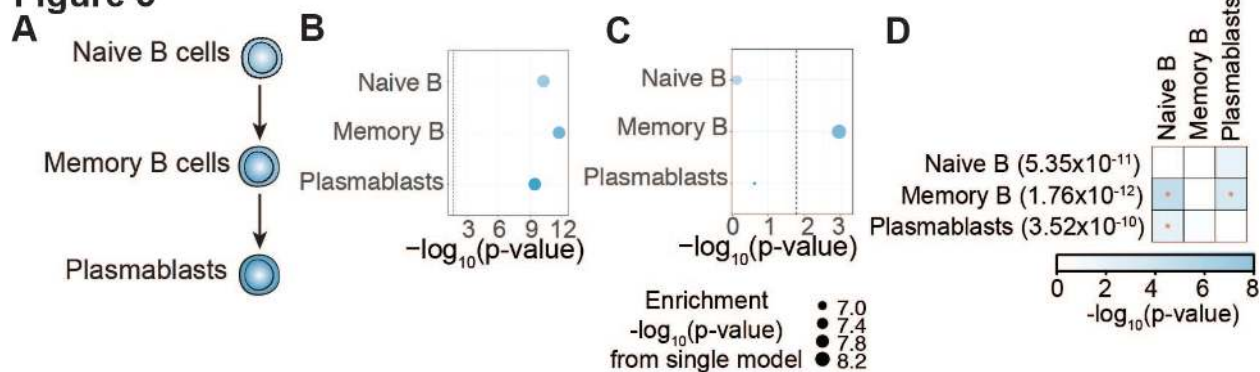
889 MS GWAS. See Figure 1B for additional description. **C:** Stratified LDSC coefficient p-values for

890 B cell lineage cell types in MS GWAS. See Figure 2A for additional description. **D:** LDSC

891 coefficient p-values for pairwise stratified analyses of MS GWAS results in ATAC-seq data from

892 B cell lineage cell types. See Figure 2B legend for additional description.

## Figure 5



893

894 **Figure 6: A:** Enrichment of MS GWAS heritability in OCRs from untreated patients with MS.

895 Enrichment p-values are shown as  $-\log_{10}(\text{p-value})$ . **B, C:** LDSC results for MS GWAS

896 enrichment in a joint model for T4cm (**B**) and cMBc (**C**) OCRs from untreated patients with MS.

897 Heights of the circles reflect stratified LDSC coefficient p-values. Sizes of the circles are

898 proportional to the enrichment p-values for that given cell type, with larger circles reflecting more

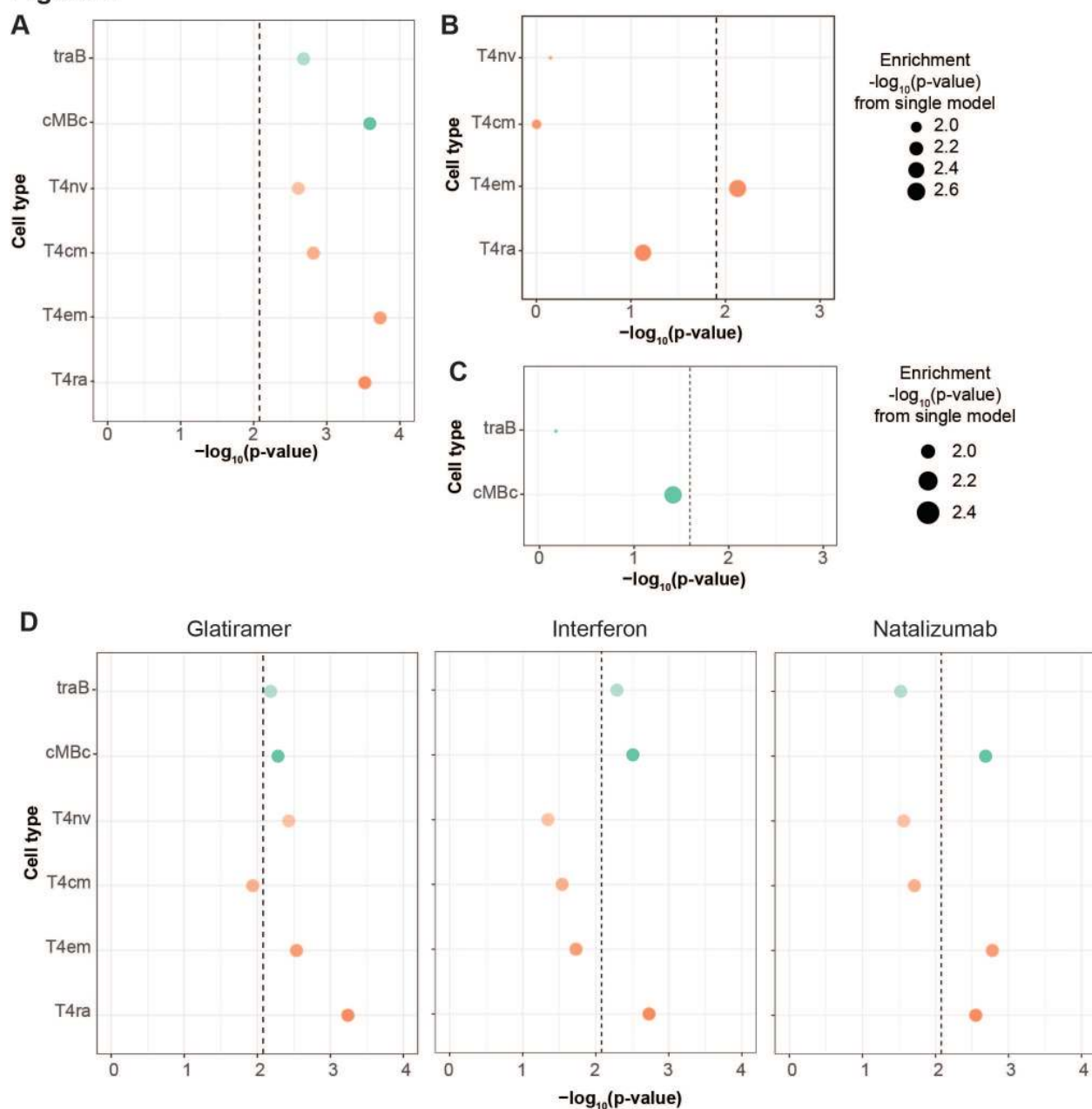
899 significant p-values. **D:** Enrichment of MS GWAS heritability in OCRs from MS patients

900 undergoing immunomodulatory treatment. Enrichment p-values are shown as  $-\log_{10}(\text{p-value})$ .

901 Treatments include glatiramer acetate, interferon, or natalizumab.



**Figure 6**



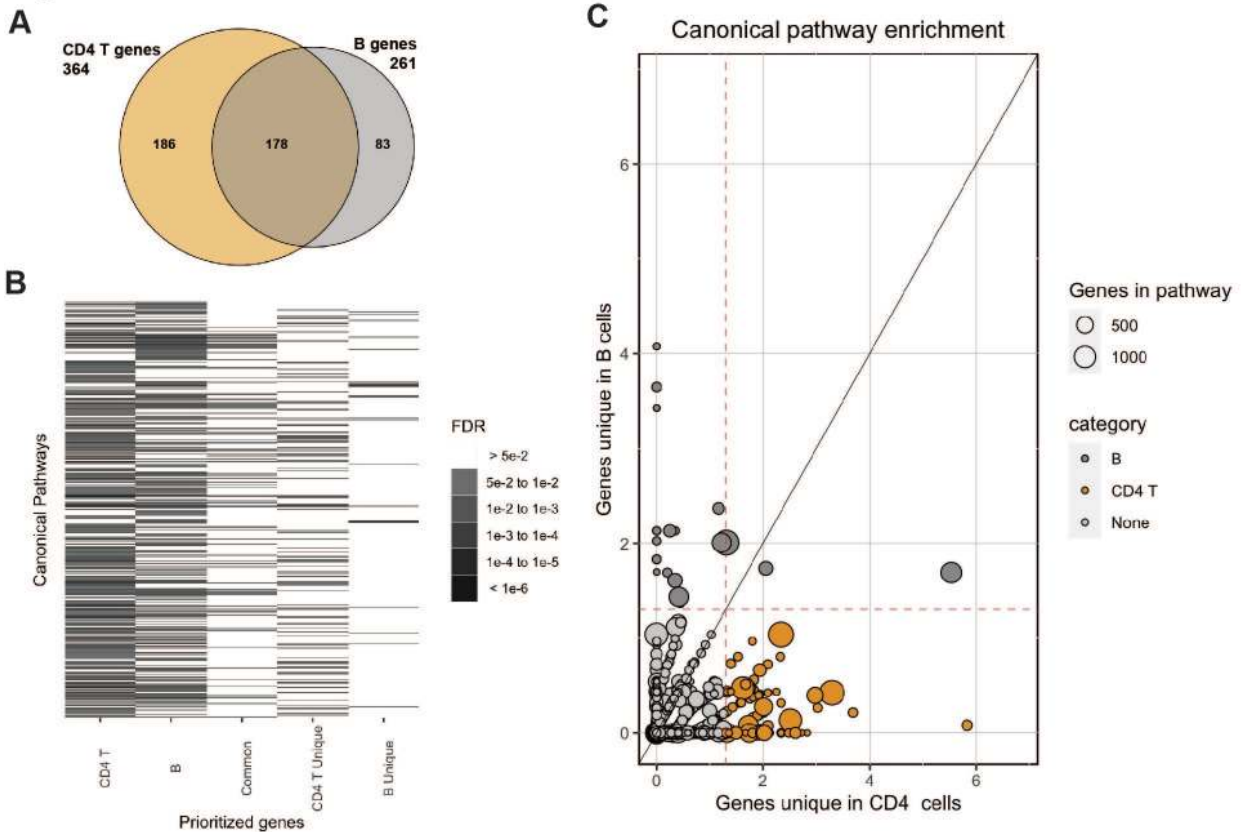
902

903

904 **Figure 7: A.** Venn diagram of the putative causal CD4 T and B cell genes. **B.** Heatmap of  
905 canonical pathway enrichment for the putative causal genes in CD4 T cells, B cells, common in  
906 CD4 T and B cells, unique in CD4 T cells, and unique in B cells. Only pathways with FDR<5% in  
907 at least one gene list are displayed (n=1950). The grayscale depicts level of statistical  
908 significance. **C.** Scatterplot of  $-\log_{10}(\text{FDR})$  of canonical pathway enrichment for putative causal

909 genes unique in CD4 T cells (X axis) vs. B cells (Y axis). The dashed red lines indicated  
 910 FDR<5%. The size of the dots depicts the total number of genes in the respective pathway.

**Figure 7**



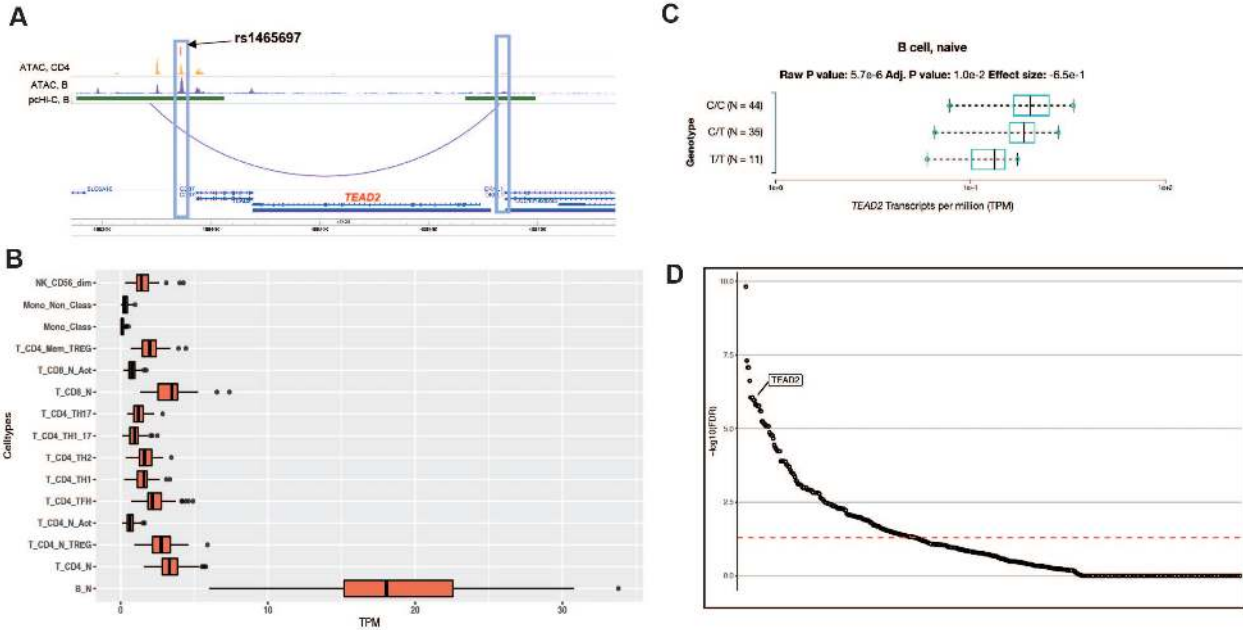
911

912

913 **Figure 8: A:** Visualization of *TEAD2* locus. Lead SNP rs1465697 (PICS of 15%) is depicted  
 914 with a red line. The blue box on the left illustrates the overlap with the ATAC-seq peaks present  
 915 in CD4 T (orange) and B cells (purple). The SNP and ATAC-seq peaks also overlap a PChIC  
 916 looping interaction with the promoter for the *TEAD2* gene (arc; the boundaries of the  
 917 enhancer/promoter regions are indicated in green; the promoter of *TEAD2* is highlighted with  
 918 the blue box on the right). **B.** Gene expression of *TEAD2* across immune cells available in the  
 919 DICE database (<https://dice-database.org/>). X axis display transcripts per million (TPM). **C.** Cis-  
 920 eQTL boxplot per genotype status of rs1465697 in naïve B cells in the DICE database  
 921 (<https://dice-database.org/>). **D.** Transcription factor enrichment in the GTRD database for the

922 putative causal genes that are common in CD4 T and B cells. Each dot represents one of 526  
 923 transcription factors. The Y axis indicates the  $-\log_{10}$  of the FDR. The *TEAD2* enrichment is  
 924 highlighted ( $p$ -value =  $1.34 \times 10^{-8}$ , FDR =  $8.81 \times 10^{-7}$ ).

**Figure 8**



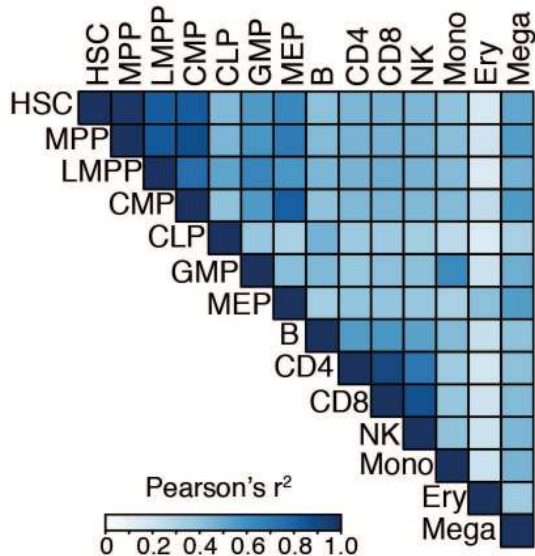
925

926

927 **Supplemental Figure Legends**

928 **Figure S1:** Correlation (Pearson's  $r^2$ ) in ATAC-seq profiles across hematopoietic cell types.

**Figure S1**

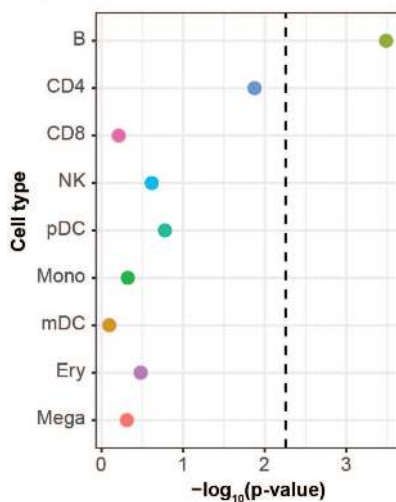


929

930

931 **Figure S2:** LDSC enrichments for MS GWAS in cell-type specific ATAC-seq peaks in each of  
932 the nine mature hematopoietic cell type. Y-axis shows  $-\log_{10}(\text{p-value})$  of the LDSC heritability  
933 enrichment.

**Figure S2**



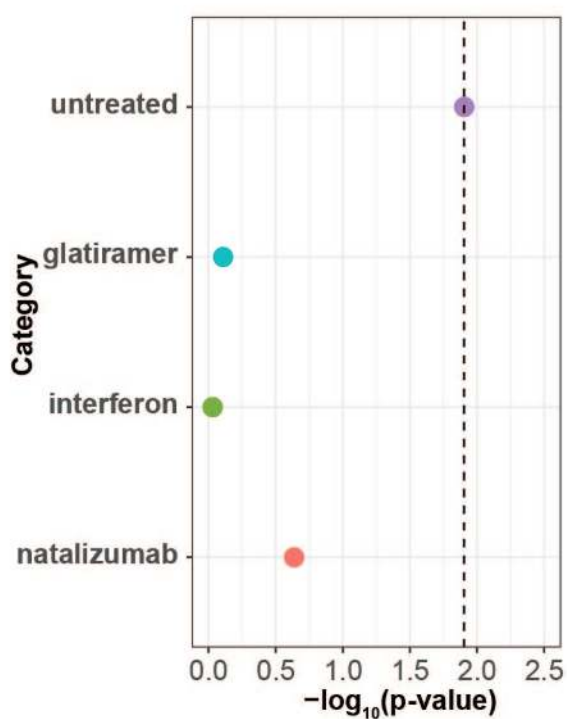
934

935

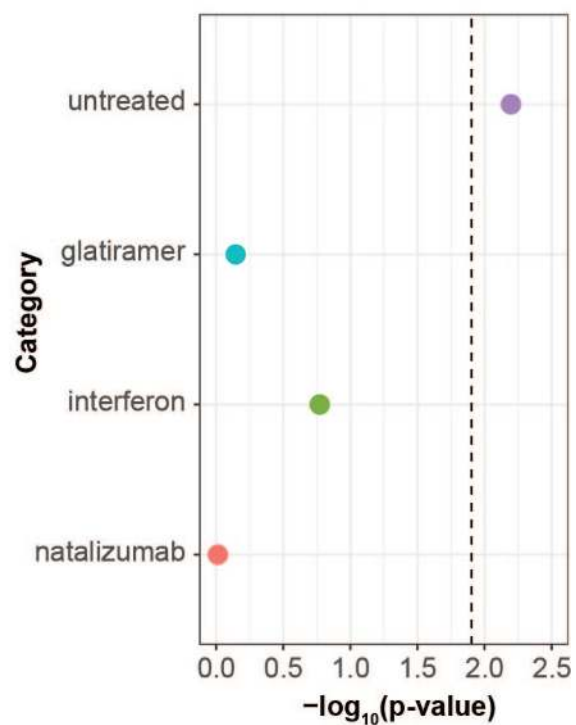
936 **Figure S3: A.** LDSC enrichment results for MS GWAS enrichment in T4cm OCRs from treated  
937 and MS treated patients in a joint model. **B.** Stratified LDSC enrichment results for MS GWAS  
938 enrichment in cMBc OCRs from treated and MS treated patients in a joint model. Heights of the  
939 circles reflect stratified LDSC coefficient p-values. Sizes of the circles are proportional to the  
940 enrichment p-values for that given cell type, with larger circles reflecting more significant p-  
941 values.

## Figure S3

A



B



942

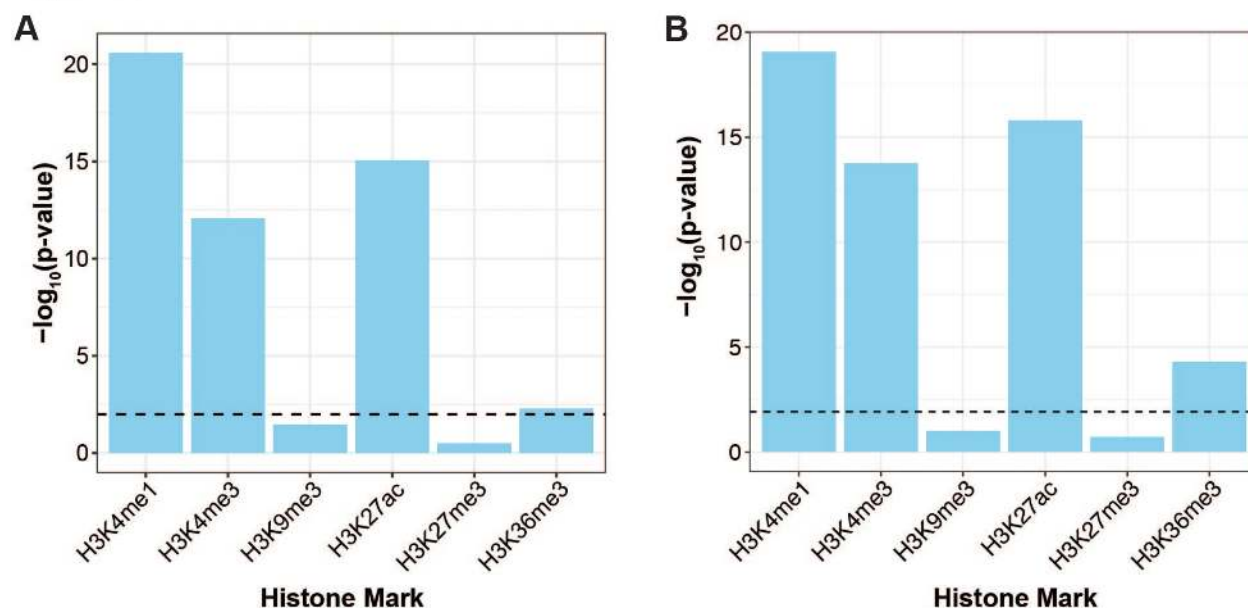
943

944 **Figure S4:** A: LDSC enrichment p-values for MS GWAS data in CD4<sup>+</sup> T cell ChIP-seq peaks of

945 various histone markers. Y-axis shown as  $-\log_{10}(\text{p-value})$ . B: Same as Figure S3A, except

946 performed for B cell ChIP-seq histone markers.

## Figure S4



947

948

949 **Figure S5: A:** LDSC enrichment p-values for chromHMM chromatin states in CD4+ T cells from

950 ENCODE. **B:** Same as Figure S5A, except for B cells from ENCODE. TssA: Active TSS;

951 PromU: Promoter Upstream TSS; PromD1: Promoter Downstream TSS 1; PromD2: Promoter

952 Downstream TSS 2; Tx5: Transcribed - 5' preferential; Tx: Strong transcription; Tx3:

953 Transcribed - 3' preferential; TxWk: Weak transcription; TxReg: Transcribed & regulatory

954 (Prom/Enh); TxEnh5: Transcribed 5' preferential and Enh; TxEnh3: Transcribed 3' preferential

955 and Enh; TxEnhW: Transcribed and Weak Enhancer; EnhA1: Active Enhancer 1; EnhA2: Active

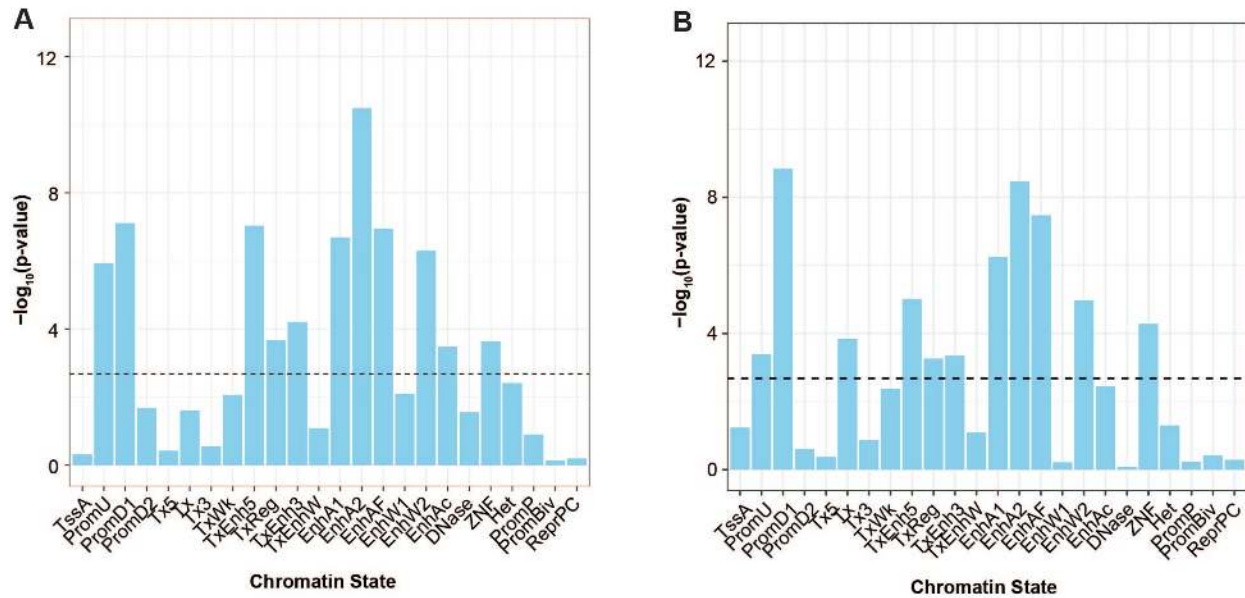
956 Enhancer 2; EnhAF: Active Enhancer Flank; EnhW1: Weak Enhancer 1; EnhW2: Weak

957 Enhancer 2; EnhAc: Primary H3K27ac possible Enhancer; DNase: Primary DNase; ZNF: ZNF

958 genes & repeats; Het: Heterochromatin; PromP: Poised Promoter; PromBiv: Bivalent Promoter;

959 ReprPC: Repressed Polycomb.

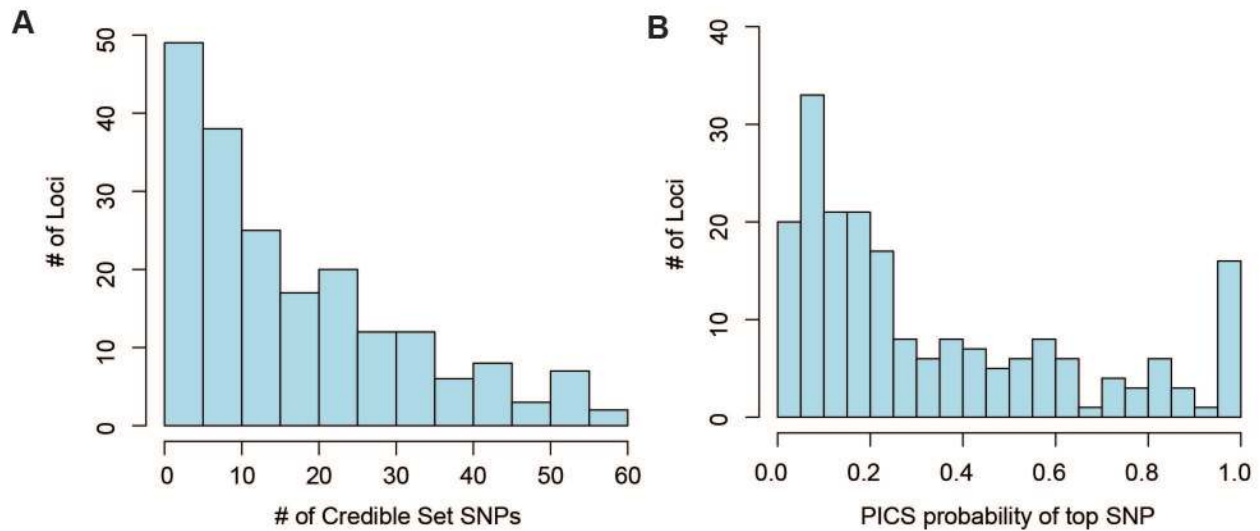
Figure S5



960

961 **Figure S6: A:** Histogram of the number of credible set (CS) variants across loci. **B:** Histogram  
962 of the PICS probability of the top variant in each locus.

Figure S6



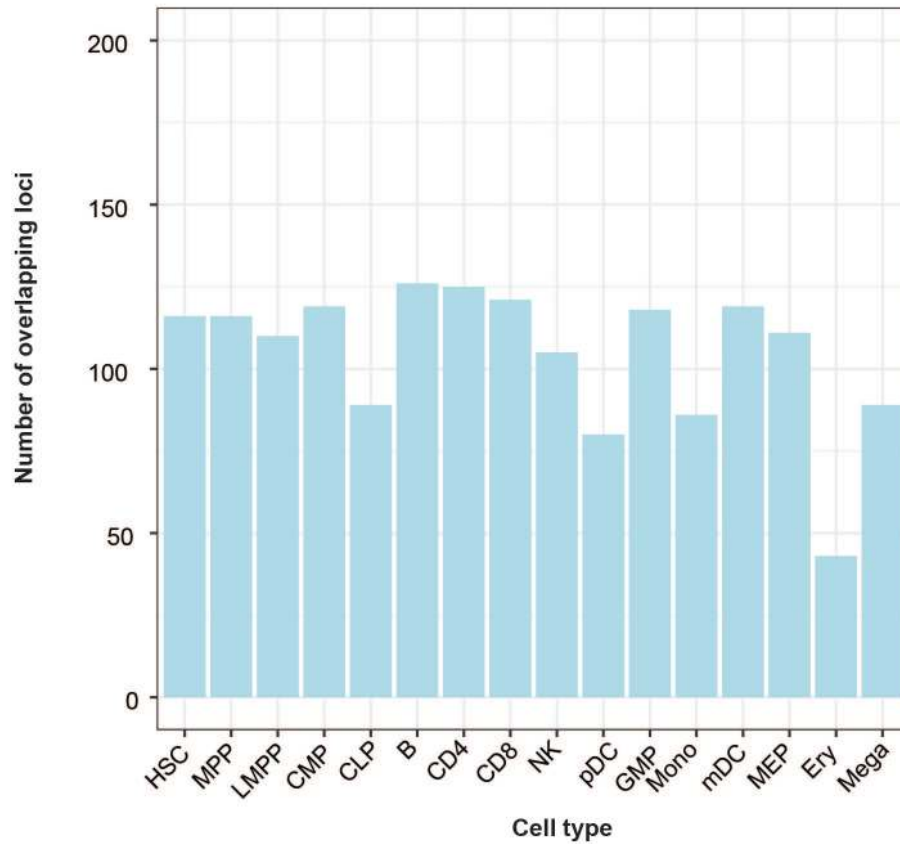
963

964

965 **Figure S7:** Number of MS GWAS loci (out of 200) with at least one CS SNP overlapping an  
966 ATAC-seq peak in the listed cell types.



**Figure S7**

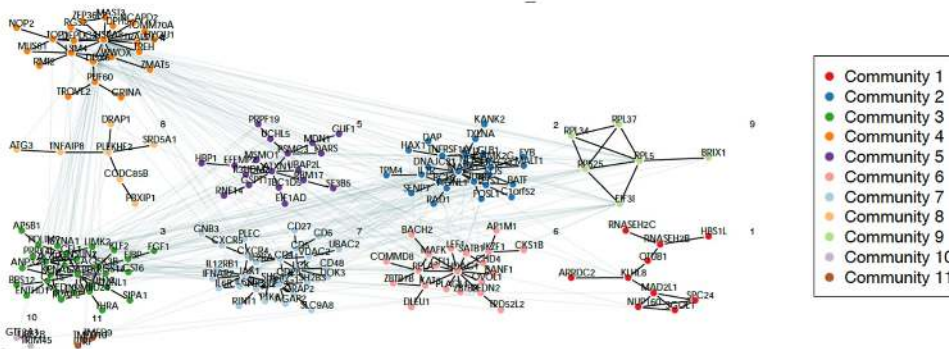


967

968

969 **Figure S8:** Protein-protein interaction communities of putative causal genes in CD4 T cells.

PPI communities of putative causal genes in CD4 T cells

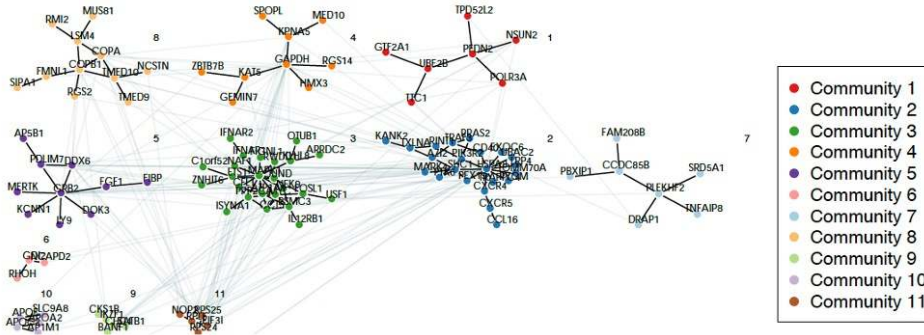


970

971 **Figure S9:** Protein-protein interaction communities of putative causal genes in B cells.



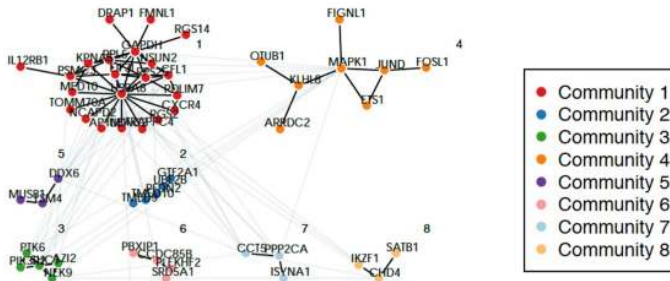
### PPI communities of putative causal genes in B cells



972

973 **Figure S10:** Protein-protein interaction communities of putative causal genes shared in CD4 T  
974 and B cells.

### PPI communities of putative causal genes common in CD4 T and B cells

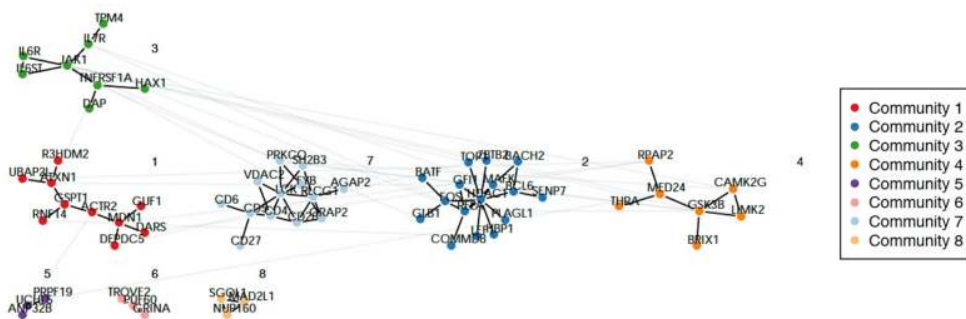


975

976

977 **Figure S11:** Protein-protein interaction communities of putative causal genes unique in CD4 T  
978 cells.

### PPI communities of putative causal genes unique in CD4 T cells



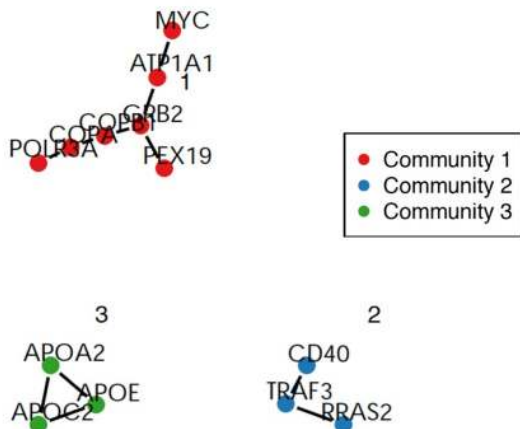
979

980

981 **Figure S12:** Protein-protein interaction communities of putative causal genes unique in B cells.

982

### PPI communities of putative causal genes unique in B cells



983

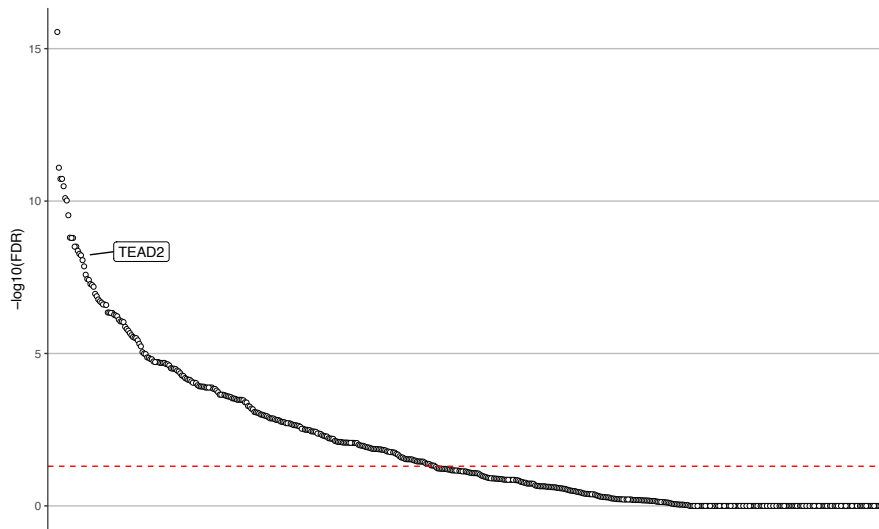
984 **Figure S13:** Enrichment of CD4 T cell putative causal genes in GTRD database. Each dot

985 represents one transcription factor. The Y axis displays  $-\log_{10}$  of false discovery rate (FDR).

986 The dashed red line indicates the threshold of 1% FDR. The enrichment for TEAD2 predicted

987 target genes is labeled.

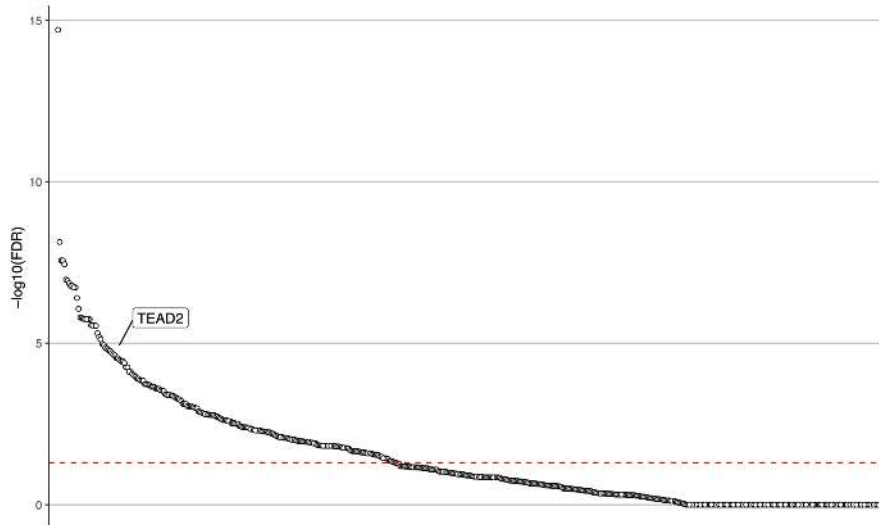
Figure S13



988

989 **Figure S14:** Enrichment of B cell putative causal genes in GTRD database. Each dot  
990 represents one transcription factor. The Y axis displays  $-\log_{10}$  of false discovery rate (FDR).  
991 The dashed red line indicates the threshold of 1% FDR. The enrichment for TEAD2 predicted  
992 target genes is labeled.

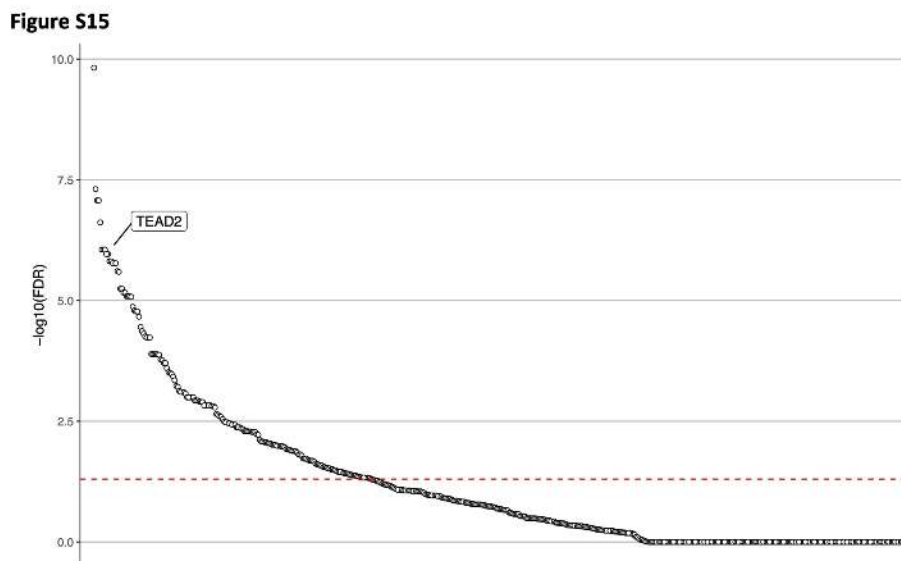
Figure S14



993

994

995 **Figure S15:** Enrichment of shared between CD4 T and B cells putative causal genes in GTRD  
996 database. Each dot represents one transcription factor. The Y axis displays  $-\log_{10}$  of false  
997 discovery rate (FDR). The dashed red line indicates the threshold of 1% FDR. The enrichment  
998 for TEAD2 predicted target genes is labeled.

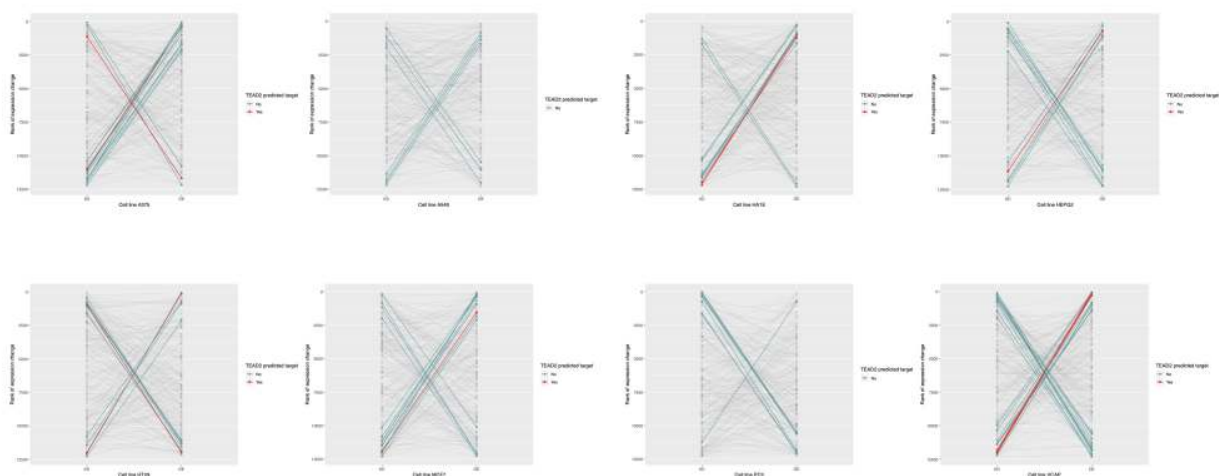


999

1000

1001 **Figure S16:** Change of gene expression of CD4 T cell putative causal genes in knock-down  
1002 (KD) and over-expression (OE) models in cancer cell lines. Eight cancer cell lines are displayed:  
1003 A375, A549, HA1E, HEPG2, HT29, MCF7, PC3, and VCAP. Putative causal genes are  
1004 represented with lines connecting the ranked KD gene expression data (left column) with the  
1005 ranked OE gene expression data (right column). Genes that are in the extreme 10% in opposite  
1006 directions are indicated with green solid lines or red solid lines if these are also a predicted gene  
1007 target for TEAD2. The light grey lines display all over putative causal genes.

**Figure S16**

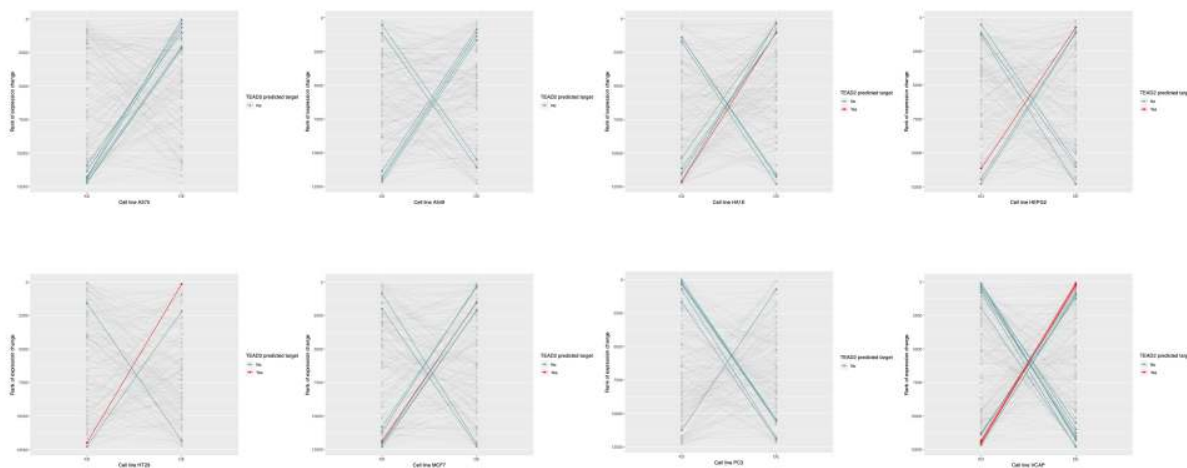


1008

1009 **Figure S17:** Change of gene expression of B cell putative causal genes in knock-down (KD)  
1010 and over-expression (OE) models in cancer cell lines. Eight cancer cell lines are displayed:  
1011 A375, A549, HA1E, HEPG2, HT29, MCF7, PC3, and VCAP. Putative causal genes are  
1012 represented with lines connecting the ranked KD gene expression data (left column) with the  
1013 ranked OE gene expression data (right column). Genes that are in the extreme 10% in opposite  
1014 directions are indicated with green solid lines or red solid lines if these are also a predicted gene  
1015 target for TEAD2. The light grey lines display all over putative causal genes.

1016

**Figure S17**



1017

1018

1019

## 1020 **Supplementary Tables**

### 1021 **Supplementary Table 1: MS GWAS enrichment in 16 hematopoietic cell types. Results**

1022 from LDSC from a model including annotation of interest and set of baseline annotations.

1023 Column 2 shows the Proportion of SNPs in OCRs of that cell type. Column 3 shows the SNP

1024 heritability ( $h^2_g$ ) for the annotation. Column 4 shows the standard error for  $h^2_g$ . Column 5 shows

1025 enrichment of SNP heritability, defined as proportion of SNP heritability in the annotation divided

1026 by the proportion of SNPs in that annotation. Column 6 shows the standard error of the

1027 enrichment of SNP heritability. Column 7 shows the p-value of the enrichment of SNP

1028 heritability.

1029

### 1030 **Supplementary Table 2: MS GWAS enrichment of hematopoietic cell types in joint model:**

1031 Results from LDSC from a joint model including annotations from all cell types and set of

1032 baseline annotations. Column 1 shows the coefficient  $\tau_c$  which measures the contribution for a  
1033 given annotation to heritability in this overall model, stratified on other annotations in the model.  
1034 Column 2 shows the standard error for the coefficient  $\tau_c$ . Column 3 shows the z-score for  
1035 coefficient  $\tau_c$  and column 4 shows the p-value for coefficient  $\tau_c$ .

1036

1037 **Supplementary Table 3. MS GWAS pairwise enrichment in 16 hematopoietic cell types.**

1038 Index cell types are shown on the left. The comparator cell types are shown on top. Coefficient  
1039 p-values are shown for the index cell type in a model that includes the index cell type,  
1040 comparator cell type, and the set of baseline annotations.

1041

1042 **Supplementary Table 4: MS GWAS cell-specific enrichment within terminal hematopoietic**

1043 **cell types.** Columns are the same as in Supplementary Table 1.

1044

1045 **Supplementary Table 5: Heritability enrichments (single model) for other disorders.**

1046 Heritability enrichment p-values for each cell types across 10 autoimmune or neuropsychiatric  
1047 disorders.

1048

1049 **Supplementary Table 6: Heritability enrichments (joint model) for other disorders.**

1050 Heritability enrichments (p-values for coefficient  $\tau_c$ ) for each cell type under joint model across  
1051 10 autoimmune or neuropsychiatric disorders.

1052

1053 **Supplementary Table 7. MS GWAS enrichment in CD4+ T cell subpopulations.** Columns

1054 are the same as in Supplementary Table 1.

1055

1056 **Supplementary Table 8. Stratified LDSC in CD4+ T cell subpopulations.** Columns are the

1057 same as in Supplementary Table 2.

1058

1059 **Supplementary Table 9. MS GWAS pairwise enrichment in CD4+ T subpopulations.**

1060 Columns are the same as in Supplementary Table 3.

1061

1062 **Supplementary Table 10. MS GWAS enrichment in B cell subpopulations.** Columns are the

1063 same as in Supplementary Table 1.

1064

1065 **Supplementary Table 11. Stratified LDSC in B cell subpopulations.** Columns are the same

1066 as in Supplementary Table 2.

1067

1068 **Supplementary Table 12. MS GWAS pairwise enrichment in B cell subpopulations.**

1069 Columns are the same as in Supplementary Table 3.

1070

1071 **Supplementary Table 13. Clinical characteristics of MS subjects.** EDSS: Expanded

1072 Disability Status Scale. \* for the Untreated subjects it indicates number of months since last

1073 treatment.

1074

1075 **Supplementary Table 14. MS GWAS enrichment across OCRs in 6 cell types isolated**

1076 **from untreated MS patients.** Columns are the same as in Supplementary Table 1.

1077

1078 **Supplementary Table 15. MS GWAS enrichment across OCRs in joint model in CD4 T cell**

1079 **types isolated from untreated MS patients.** Columns are the same as in Supplementary

1080 Table 2.

1081



1082 **Supplementary Table 16. MS GWAS enrichment across OCRs in joint model in B cell**  
1083 **types isolated from untreated MS patients.** Columns are the same as in Supplementary  
1084 Table 2.

1085  
1086 **Supplementary Table 17 MS GWAS enrichment across OCRs in 6 cell types isolated from**  
1087 **treated MS patients.** Columns are the same as in Supplementary Table 1, except column  
1088 added for the immune-modulating treatment

1089  
1090 **Supplementary Table 18. MS GWAS enrichment across OCRs in joint model in T4em**  
1091 **isolated from untreated and treated MS patients.** Columns are the same as in  
1092 Supplementary Table 2

1093  
1094 **Supplementary Table 19. MS GWAS enrichment across OCRs in joint model in cMBc**  
1095 **isolated from untreated and treated MS patients.** Columns are the same as in  
1096 Supplementary Table 2

1097  
1098 **Supplementary Table 20. MS GWAS enrichments in histone ChIP-seq from T<sub>h</sub>17 cells.**  
1099 Columns are the same as in Supplementary Table 1.

1100  
1101 **Supplementary Table 21. MS GWAS enrichments in histone ChIP-seq from B cells.**  
1102 Columns are the same as in Supplementary Table 1.

1103  
1104 **Supplementary Table 20. MS GWAS enrichments in chromatin states from T<sub>h</sub>17 cells.**  
1105 Columns are the same as in Supplementary Table 1.

1106

1107 **Supplementary Table 21. MS GWAS enrichments in chromatin states from B cells.**

1108 Columns are the same as in Supplementary Table 1.

1109

1110 **Supplementary Table 24: Summary of gene prioritizations.** For each GWAS locus, the lead

1111 SNP ("Effect SNP"), region annotation according to Patsopoulos et al., lead SNP chromosome,

1112 lead SNP position (in hg19), A1 allele, A2 allele, odd's ratio (OR) and lead SNP p-value are

1113 shown. Previous gene prioritizations from Patsopolous et al., based on various criteria are

1114 listed. For columns "B Cell ATAC (Buenrostro)", "B Cell ATAC (Calderon)", "Memory B Cell

1115 ATAC (Calderon)", "CD4 Cell ATAC (Buenrostro)", "CD4 Cell ATAC (Calderon)", "Th17 Cell

1116 ATAC (Calderon)", a "1" indicates that a credible set SNP in the locus directly intersects an

1117 OCR from the indicated ATAC-seq dataset ("0" if no credible set SNP in the locus directly

1118 intersects. "PCHiC CD4 genes" and "PCHiC B genes" columns list genes that have a promoter

1119 capture HiC looping interaction to a credible set SNP in the indicated cell type. "PCHiC + ATAC

1120 CD4 genes" indicates a credible set SNP intersect an OCR in CD4 T cells and forms a PCHiC

1121 looping interaction in CD4 T cells to that gene. "PCHiC + ATAC B genes" indicates a credible

1122 set SNP intersect an OCR in B cells and forms a PCHiC looping interaction in B cells to that

1123 gene. The number of credible set SNPs in each locus is shown in the last column.

1124

1125 **Supplementary Table 25: Canonical pathway enrichment for prioritized MS genes.**

1126

1127 **Supplementary Table 26: Protein-protein interaction connectivity summaries for**

1128 **prioritized gene lists.** Detailed outputs from GeNets are provide.

1129

1130 **Supplementary Table 27: CD4 T prioritized genes ranked in the opposite extreme 10% of**

1131 **gene expression changes in KD and OE cell lines.**

1132

1133 **Supplementary Table 28: B prioritized genes ranked in the opposite extreme 10% of gene**  
1134 **expression changes in KD and OE cell lines.**

1135

1136 **Supplementary Table 29: Markers for FACS sorting strategy of Verily ATAC-seq data**

1137

1138